Ab initio Mechanistic Investigation for the Formation of In-MOFs

by

Vincent T. DelFratte

Submitted in Partial Fulfillment of the Requirements

for the Degree of

Master of Science

in the

Chemistry

Program

YOUNGSTOWN STATE UNIVERSITY

August, 2023

Ab initio Mechanistic Investigation for the Formation of In-MOFs

Vincent T. DelFratte

I hereby release this thesis to the public. I understand that this thesis will be made available from the OhioLINK ETD Center and the Maag Library Circulation Desk for public access. I also authorize the University or other individuals to make copies of this thesis as needed for scholarly research.

Signature:

_____

Vincent T. DelFratte, Student   Date

Approvals:

_____

Dr. Douglas Genna, Thesis Advisor   Date

_____

Dr. Christopher Arntsen, Committee Member   Date

_____

Dr. Brian Leskiw, Committee Member   Date

_____

Dr. Salvatore A. Sanders, Dean of Graduate Studies   Date

Acknowledgements

I would like to thank my thesis advisor, Dr. Douglas Genna, for his unwavering support throughout the past three years. Dr. Genna is a wonderful example of not just a great instructor and researcher, but also a mentor and role model. I am blessed to have been a part of his research group, as I have gained so much invaluable knowledge and experience. His expertise, scientific insight, and love for chemistry has made it difficult to not become excited when discussing the subject, and it reminds me why I remain a part of this field of study.

I also extend my thanks to the entire Genna Lab. Never did I think I would become close to (let alone get the opportunity to work alongside) such a talented group of individuals. The highlight of my week always fell on "group meeting"—it was the reason I got through the week most times. I know everyone will continue to do great things, and I wish them luck in all their endeavors.

I'd also like to take the opportunity to thank my best friends Jake, Jake, Victoria, and Aurelia. They have been there to listen and give me feedback on everything that has ever been thrown my way. I genuinely wouldn't trade them for anything in the world, and words cannot express how much they all mean to me.

I would finally like to thank my parents and sister (and Tucker) for continually being there for me even when I have doubted myself. They have all sacrificed the most to ensure that I excel at everything I set forth doing, and their unconditional love and support is the reason I keep going. I couldn't have done any of this without them, and for that I am forever grateful.

Abstract

Herein, density functional theory (DFT) was used for optimizing the geometry of proposed intermediates, built using Spartan Student, in the synthesis of the indium infinite-chain secondary building unit. Dimeric indium species with similar backbones were proposed for each system as a representative of the indium infinite-chain secondary building unit. By calculating the enthalpies of formation for intermediates created from $InCl_3(H_2O)$ and $In(NO_3)_3(H_2O)$, similar and contrasting enthalpic trends between systems and individually proposed mechanisms were found and compared. All systems consist of motifs 1, 2, 3a, and 3b, which attempt to describe similar mechanistic routes from starting material to proposed dimer. The deprotonation of water before and after becoming a μ^2 bridge with respect to two indium atoms was compared among systems, and the most enthalpically favorable bridge to form first (hydroxyl or carboxylate) in the synthesis of the indium infinite chain secondary building unit was examined. After analyzing the results, they support the possibility that there may be multiple enthalpically reasonable methods of self-assembly and repair.

Table of Contents

I. Introduction

Metal-Organic Frameworks (MOFs)

Metal-organic frameworks (MOFs) are porous, crystalline coordination polymers[1,2]. These materials are formed when organic linkers (typically polytopic carboxylic acids) and metal clusters, atoms, or ions (referred to as nodes) coordinate to one another[3,4]. The result of this coordination is either a 2D or 3D extended framework. Yaghi first employed the term "metal-organic framework" in the late 1990s, along with his colleagues, where they published one of the first reports of a material that could maintain porosity without the presence of guest molecules[1].
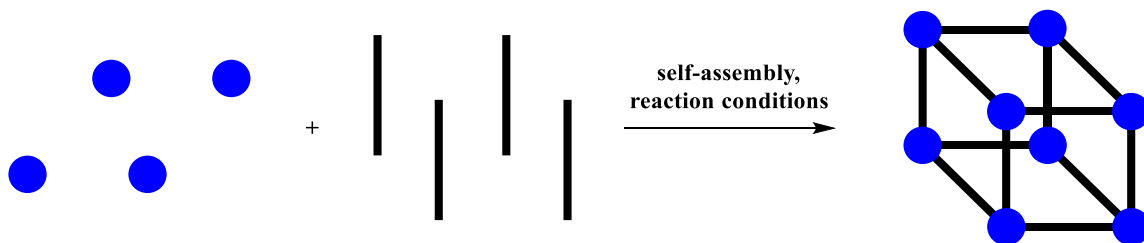

Scheme 1. A cartoon depiction of self-assembly of MOFs. Blue circles represent nodes and black lines represent organic linker.

While a MOFs geometry is dependent on the secondary building unit (SBU), the SBU is dependent on the chemical makeup of its molecular building unit(s) (MBUs)[5]. MBUs are discreet molecular substructures formed during self-assembly, and oftentimes can be synonymous with prenucleation building units (PNBUs); definitionally, these can be any molecular species that accumulate prior to nucleation due to thermodynamic or kinetic boundaries[6,7]. As a result of many moving parts, there is a cascade of building steps all of which rely heavily on a MBU to MOF model.

Given the vast number of metals, oxidation states, and organic linkers, there is a vast number of possible SBUs and MOFs that can be synthesized[8–10]. MOFs have become an increasingly attractive field to chemists because of their functionality and ability to be altered to fulfill a specific task[2,11,12]. Since there is such a myriad of interchangeable metals and organic linkers, it is desirable to investigate the various combinations with the hope of finding new uses and improving upon already existing MOFs. With this in mind, MOFs have already been applied to various applications that include gas storage, drug delivery, sensing, catalysis, and water remediation (a topic that has been investigated by the Genna lab)[13–17].

Indium Derived MOFs

Trivalent group 13 metals are often utilized in MOF chemistry, because metal salts made from aluminum (Al), gallium (Ga), and indium (In) provide a naturally electron-rich environment for ligands to bond, and allow for various coordination complexes to be formed[18,19]. Indium is an attractive +3 metal because it can take on a wide range of charges, aforementioned coordination modes, and has the ability to bind up to seven ligands (depending on steric interactions and ligand type)[20]. In-MOFs are made from some of the most common SBUs among +3 metals[21,22]. These SBUs include an anionic metal-tetracarboxylate, a cationic metal-trimer, and the neutral infinite chain shown in **figure 1**.
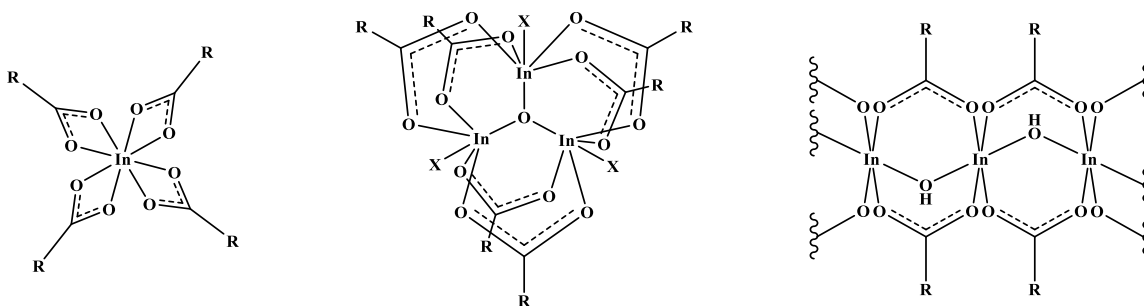
Figure 1. The anionic tetracarboxylate In-SBU, cationic In-trimer SBU, and neutral In-infinite chain SBU. R-groups represent polytopic carboxylate linker and X-groups represent capping ligands.

The infinite chain is an SBU in which metal atoms are bridged by ligands that allow the structure to extend infinitely along a single Cartesian axis, while additional ligands allow for the structure to become 3-dimensional. Primary examples are MIL-68(In) and MIL-53(In) (MIL= Matériaux de l′Institut Lavoisier), both of which are compromised of the infinite chain and terephthalate. MIL-68(In) was first synthesized by Volkringer in 2008[23]. MIL-68(In) is reported as having a 3D network with a Kagome-type topology. The

structure is made of infinite, unidirectional trans connected chains with octahedral

$InO_4(OH)_2$ centers. These chains are further coordinated to one another using terephthalate.

As a result of this coordination, unidirectional triangular and hexagonal pore channels are

present (**figure 2**).

Figure 2. A portion of MIL-68(In) showing the chemical makeup of the infinite chain SBU. Triagonal and hexagonal pores are made from the coordination of In-atoms (blue), terephthalate oxygen (red), and hydroxide (red). Hydrogens are omitted for clarity.

Self-Assembly of Molecular Indium

The process in which MBUs, nodes, and organic linkers coordinate with each other

is through reversible self-assembly[24,25]. Self-assembly is accepted by MOF-chemists as the

growth and repair mechanism for MOFs; however, a detailed understanding of self-

assembly in molecular species is not well understood and the intermediates contained to

the reaction solution remain a mystery. Knowing the solution-state intermediates in a MOF

synthesis may lead to better control over a seemingly unpredictable assembly with

inconsistent reproducibility. Additionally, a mechanistic understanding of SBU formation

could aid in molecular precision and controlled multistep syntheses of new and existing materials[26]. When creating novel MOFs with unique characteristics, high surface area and porosity are just some of the qualities highly sought after; therefore, understanding SBU formation from a mechanistic standpoint could lead to the deliberate design of future materials with better attributes[27].

The determination of possible mechanisms and intermediates used in the self-assembly of MOFs revolves around multiple methods of spectroscopy, synthesis, and computation. Given how In-atoms are bridged via carboxylate and hydroxide in the infinite chain, it can be hypothesized that the *In-atoms are joined by either an initial carboxylate or hydroxide bridge which precedes additional self-assembly*. Understanding the initial bridge formation could be integral to the self-assembly process, and may be used to redeem stalled self-assembly processes during MOF synthesis.

Feng and Bu have previously proposed that the infinite chain and cationic trimer In-SBUs are dependent on the same early stage MBU(s) (or PNBUs), and a solution equilibrium dictates which can coexist[21]. They have suggested that an In-dimer intermediate is a bridge point between the cationic trimer or, more structurally similar, the infinite chain. As a common intermediate, metal-monocarboxylate is a promising MBU that has been proposed for infinite-chain derived MOFs and intermediates. Distaso has proposed the assignment of Al-monocarboxylate as a potential PNBU, based on time-resolved Raman and infrared (IR) spectroscopy values from literature[7]. While investigating the mechanism of formation for the self-assembly of MIL-53(Al), a MOF analogous with MIL-53(In), she has provided data which she suggests shows an Al-monocarboxylate PNBU accumulation that grows in solution and ultimately forms the Al-infinite chain

SBU[28,29]. This is of great importance because aluminum and indium come from the same periodic group, and both metals may share similar coordination characteristics.

Ab initio Self-Assembly

In addition to her experimental work, Distaso has performed computational analysis of SBU self-assembly for MIL-53(Al) in an attempt to disclose the "true" mechanism of action. The work suggests that MIL-53(Al) forms from $[Al(H_2O)_6]^{3+}$ via the conversion of all starting material to Al-monocarboxylate[30]. Her computational methods consist of modeling the activation energy of Al-monocarboxylate formation, with the addition of concurrent equivalents of Al-monocarboxylate, to form MIL-53(Al). The energies were calculated using her own in-situ Raman bands collected during MOF growth, and by using the aid of previously known Al-carboxylate band values as a guide. What she determined was that the activation energy of forming the Al-monocarboxylate from $[Al(H_2O)_6]^{3+}$ and organic linker is 24.9 kJ/mol less than the formation of MIL-53(Al) from Al-monocarboxylate. This suggests that before the chain begins to form, there could be an accumulation of the Al-monocarboxylate PNBU because of a possibly high kinetic barrier leading to later stage self-assembly.

Lee has also supported metal-monocarboxylate as the PNBU synthesized during the self-assembly of MIL-68(In); this was performed using literature values and computational results published by Glezakou[31,32]. In the work performed by Glezakou, he used molecular dynamics to determine how Cr-atoms and terephthalate interact to create partially formed MIL-101(Cr) SBUs (a MOF that has an isomeric Cr-trimer SBU analogue similar to the In-trimer SBU)[32]. Glezakou hypothesized that the elementary interactions in solution consist of single Cr-atoms reacting with the terminal oxygens of partially

6

deprotonated terephthalic acid. This hypothesis can be related to the proposal by Feng and Bu where they hypothesized about an equilibrium between In-SBUs in solution[21]. Because monomeric indium can form both infinite chains and trimer, and it is proposed that the infinite chain and trimer have a common intermediate, then they should both be dependent on the same early stage intermediate(s), that being In-monocarboxylate.
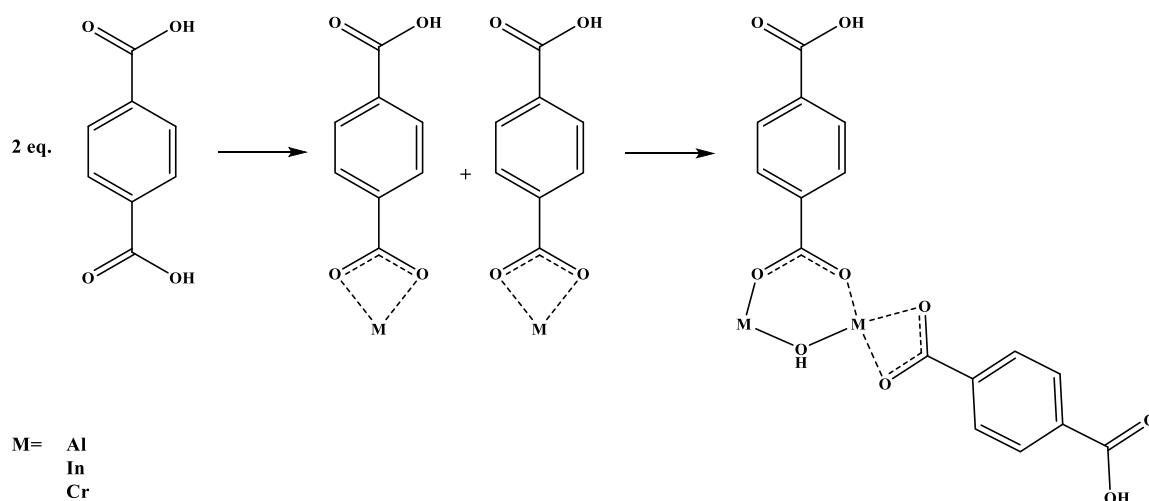
Scheme 2. Metal-monocarboxylate formation and coordination as previously proposed by Distaso, Lee, and Glezakou[30–32].

In this work, I am proposing four general motifs that attempt to describe the bridge forming sequences as follows:

Motif 1. Coordinated water forms a μ^2 bridge between In-atoms and is followed by deprotonation. Successive addition and coordination of two formate molecules create the second and third bridge.

2 eq. InX$_3$(H$_2$O)

X= Cl
NO$_3$
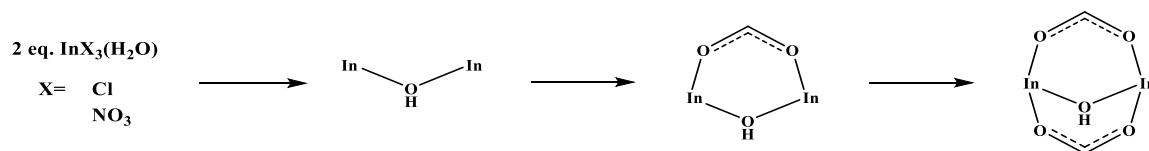
Scheme 3. Schematic representation of motif 1. Other intermediates/steps, shed ions, and coordinatively saturating ligands have been omitted for clarity.

Motif 2. Partial conversion of the starting material to In-monocarboxylate occurs, which initiates dimerization. Water forms a μ^2 bridge between In-atoms and is followed by deprotonation; it is at this point where motifs 1 and 2 converge on a common intermediate. The addition and coordination of one formate molecule creates the third bridge.

InX$_3$(H$_2$O)

X= Cl
NO$_3$
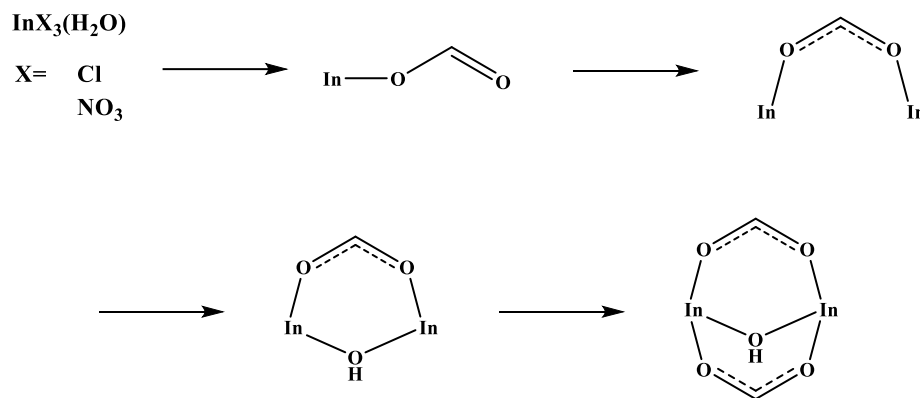
Scheme 4. Schematic representation of motif 2. Other intermediates/steps, shed ions, and coordinatively saturating ligands have been omitted for clarity.

Motif 3a. Total conversion of starting material to In-monocarboxylate occurs. Both equivalents dimerize via one of the In-formate bonds. The other coordinated formate creates a second bridge, and is proceeded by the coordination and deprotonation of a μ^2 water bridge.

Scheme 5. Schematic representation of motif 3a. Other intermediates/steps, shed ions, and coordinatively saturating ligands have been omitted for clarity.

Motif 3b. Like motif 3a, total conversion of starting material to In-monocarboxylate occurs. Both equivalents dimerize via one of the In-formate bonds. Water forms a μ^2 bridge between In-atoms and is followed by deprotonation; it is at this point that motif 1, 2, and 3b converge on a common intermediate.

2 eq. InX$_3$(H$_2$O)

X=   Cl
     NO$_3$

2 eq.   In—O ... O

In   In
            OCHO

In   In
   O
   H   OCHO

In   In
   O
   H

Scheme 6. Schematic representation of motif 3b. Other intermediates/steps, shed ions, and coordinatively saturating ligands have been omitted for clarity.

We can use these motifs and computational methods to calculate "snapshot" energies of discreet molecular species and further hypothesize if certain intermediates are enthalpically relevant. Previous computational studies performed by Genna regarding the anionic In-tetracarboxylate SBU involves these types of calculations[22]. The method developed includes a "roadmap" of proposed intermediates ranging from neutral to dianionic. Of those intermediates, seven have been synthesized and isolated, which helps pair computational results and experimental procedures. Using molecular modeling and Q-chem for finding optimized structures, Hess's Law can be used to subtract the total enthalpy of reactants from the total enthalpy of products; the calculated enthalpies of formation can be compared to proposed mechanistic pathways to support or deny their feasibility. This method of computation and analysis has provided useful insight into the possible intermediates that are a part of the reaction solution during the synthesis of anionic In-MOFs; therefore, I have employed a similar computation-based approach to elucidate possible intermediates in the formation of the In-infinite chain SBU. The proposed intermediates along the reaction coordinates summarized in motifs 1, 2, 3a and 3b will be

explored with both $InCl_3$ and $In(NO_3)_3$ containing systems. The enthalpies of formation of the individual reaction coordinates will be calculated and compared to determine if one motif is preferred over another.

I.   Methodology

All solution-phase DFT calculations were performed using the 6-31G* basis set for all organic atoms, while the LANL2DZ-SV basis set was used for In atoms. The ωB97X-D functional was used for both organic and inorganic atoms. These decisions were based off previous methodology from the Genna lab in which similar structures were made[22]. All molecules were built using Spartan Student v8 and had their geometry preliminarily minimized using the in-program optimization feature. Formate was used in place of terephthalate as a computationally affordable alternative, and all linkers were assumed deprotonated from the start. Additionally, the loss of charged ligands (i.e., chloride and nitrate) were assumed to be free ions in solution. The molecular coordinates of all species were extracted and submitted to Q-chem for final optimization.

Initial calculations for proposed intermediates with In-Cl bonds were performed using $InCl_3(H_2O)$ (**I**) as the starting material. **I** was primarily used in the beginning of this project because it lacks the complexity of other systems, and was easier to manipulate while becoming acclimated to the Linux user-interface and workflow. Once submitted jobs were completed, the optimized coordinates were reinserted into Spartan Student as XYZ files for structural analyzation. The raw enthalpy values at 298.15 K were used to determine the relative enthalpy of each intermediate. Hess's Law was used in determining this, and so the raw output values of starting material and other reactants were summed and subtracted from the summation of each product's output enthalpies. All enthalpies reported in the results section are relative to their system's respective starting material (either **I**, **II**, or **III,** all pictured in **figure 3**).
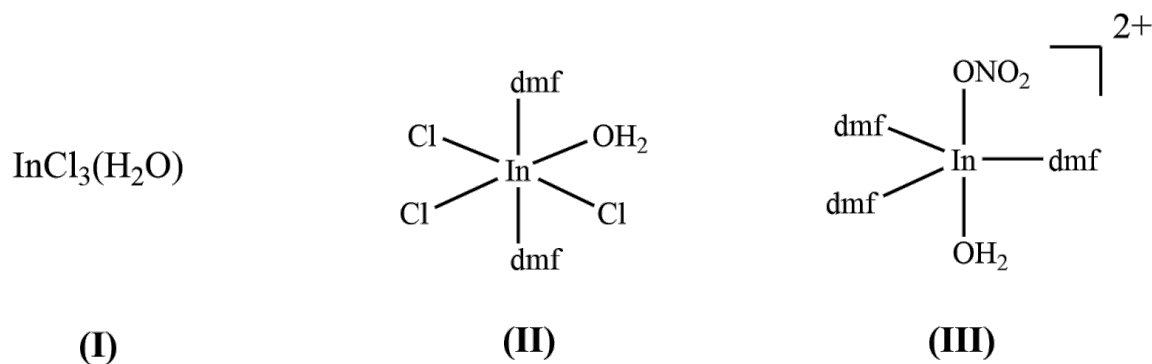
Figure 3. Starting materials for the unsolvated $InCl_3(H_2O)$ system (**I**), solvated $InCl_3(H_2O)$ system (**II**), and solvated $In(NO_3)_3(H_2O)$ system (**III**).

After analyzing the unsolvated $InCl_3(H_2O)$ system, further calculations were conducted using **II** as the starting material. **II** was chosen as the starting point for all solvated $InCl_3(H_2O)$ derived mechanisms since DMF solvation is enthalpically favored. The proposed structure of **II** is supported by the octahedral crystal structure of a previously isolated dioxane solvate that contains the coordination of two dioxane solvent molecules to the central In-atom[22]. Additionally, In-DMF bands have been detected by *in situ* Raman spectroscopy[22].

Alongside calculations involving solvated $InCl_3(H_2O)$, the solvated $In(NO_3)_3(H_2O)$ system was explored. Single crystal X-ray diffraction (SCXRD) reveals the structure of solid-state $In(NO_3)_3(H_2O)$ to be $[In(NO_3)(H_2O)_5]^{2+}$ with two counter-balancing nitrates in the outer sphere[33]. Moreover, Raman spectroscopy confirms that one of the main species in aqueous $In(NO_3)_3(H_2O)$ solution is $[In(NO_3)(H_2O)_5]^{2+}$[34]. For the solvation of this species in DMF instead of an aqueous environment, four water ligands were replaced with DMF ligands. The fifth In-water bond remained intact out of convenience— it would be counterintuitive to replace water with a DMF ligand and then reinsert exogenous water.

Using seven-coordinated indium as the starting material proved to be complicated, however. When DFT calculations were performed, the optimization equilibrium would time out and no minima could be found. This is most likely due to steric interferences from the four large DMF ligands per In-atom. To allow the optimization of intermediates to complete, the coordination number of $[In(NO_3)(DMF)_4H_2O]^{2+}$ was reduced to six by removing a DMF ligand. Doing so causes the In-atom to become strained-octahedral with the final formula $[In(NO_3)(DMF)_3H_2O]^{2+}$ (**III**). Unfortunately, even with this reduced coordination sphere, a majority of the molecules proposed for the solvated $In(NO_3)_3(H_2O)$ system still contained an exceedingly high degree of freedom. As a result, there would be no way for the molecule to appropriately converge. To circumvent this issue, certain atomic cartesian coordinates had to be constrained. These atoms consisted of the coordinates of similar atoms from corresponding, optimized structures from the solvated $InCl_3(H_2O)$ system (i.e., the In-atoms and atoms which formed H_2O, OH, and formate bridges). They were used as a foundation for building the rest of the intermediate(s). Constraining the coordinates of these atoms served as a model that would give the most accurately approximated starting point geometry.

II.   Results

Unsolvated InCl₃(H₂O) System

Pathway 1

The first proposed mechanism involves the dimerization of two molecules of **I** via bound water. The indium center that will be "donating" the water will be referred to as In$_A$, while the indium center "accepting" the water will be referred to as In$_B$. The product of bridging each In-atom with water is intermediate **IV** (H= -7.3 kcal/mol). Exogenous formate is then used to deprotonate the bridging water to form **V** (H= -54.6 kcal/mol). The loss of chloride from In$_B$ that follows forms **VI** (H= -24.8 kcal/mol), and the binding of κ^1 formate to In$_B$ forms **VII** (H= -77.6 kcal/mol). This intermediate is followed by the formation of **VIII**, which is the product of the κ^1 formate bridging both In-atoms (H= -86.6 kcal/mol). **IX** is produced upon the loss of a chloride ligand from In$_A$ (H= -60.9 kcal/mol). Another equivalent of formate is bound to In$_A$ as a κ^1 ligand which ultimately forms **X** (H= -108.6 kcal/mol). When the formate bridges in the next step, it creates **XI** (H= -118.4 kcal/mol). The last step is the loss of chloride from In$_B$; this forms the unsolvated dimer **XII** (H= -91.7 kcal/mol).
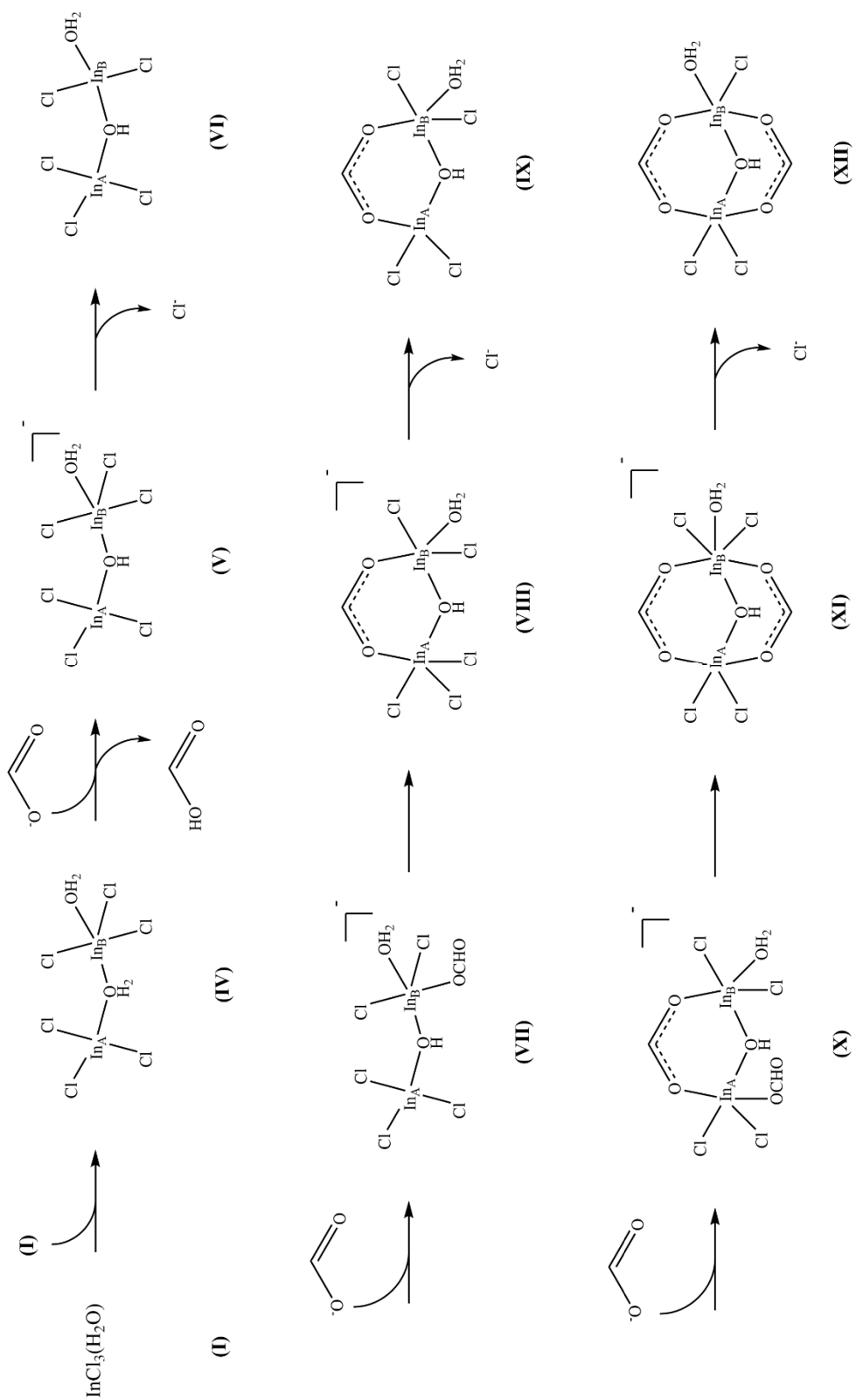
Scheme 7. The proposed mechanism of formation for **XII** as suggested by motif 1 of the unsolvated InCl₃(H₂O) system.

16
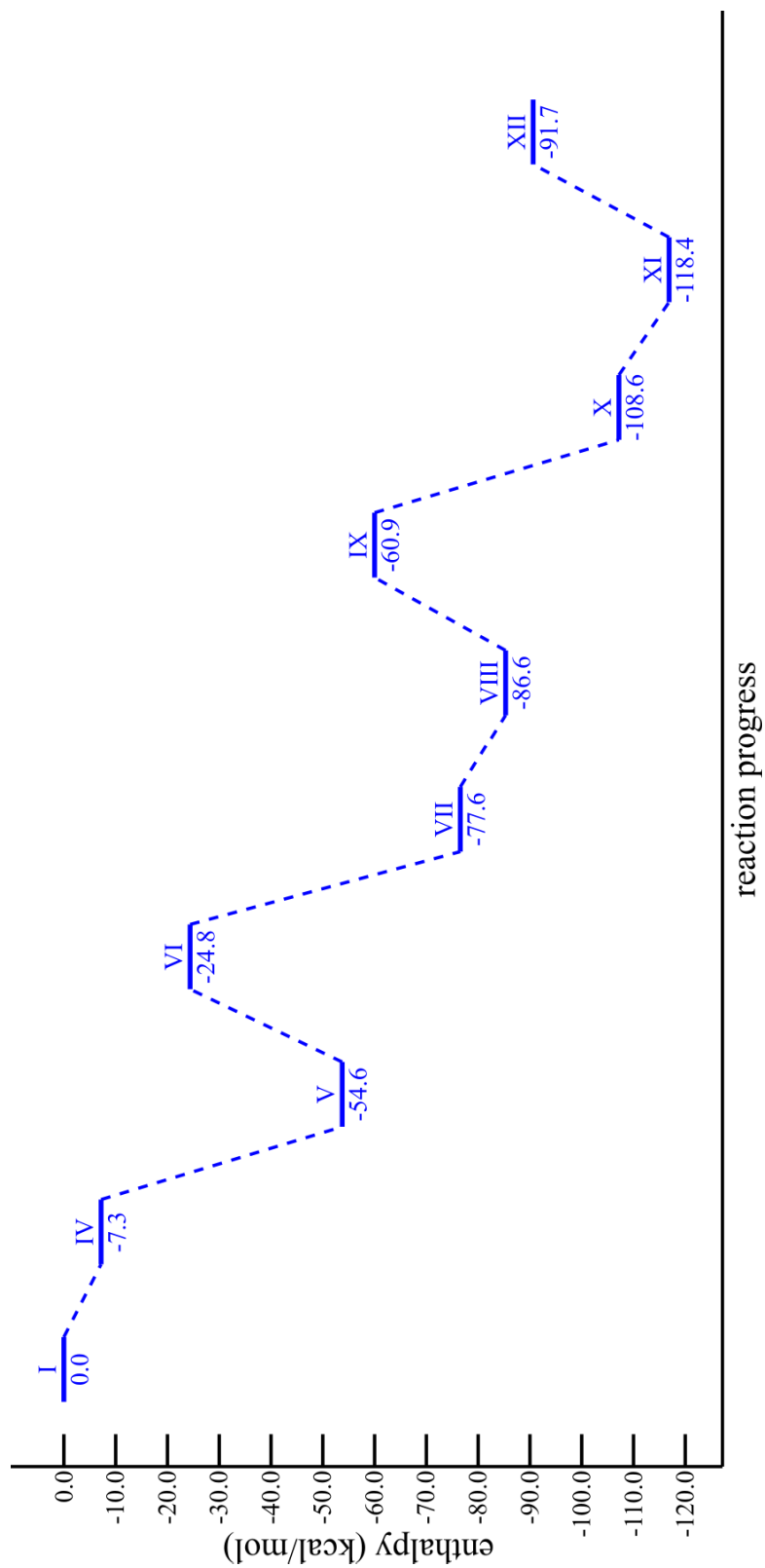
Figure 4. The energy profile diagram for pathway 1 of the unsolvated $InCl_3(H_2O)$ system plotted as reaction progress (X-axis) versus the relative enthalpy of formation (Y-axis).

Pathway 2

Mechanism 2 begins by producing one equivalent of In-monocarboxylate via formate and **I**. The In-monocarboxylate made, **XIII**, has an enthalpy of -39.0 kcal/mol. This is the source of In_A. Another equivalent of **I**, the source of In_B, will "accept" the formate from the In-monocarboxylate formed in the prior step. This reaction forms **XIV** (H= -67.4 kcal/mol). In_B then sheds a chloride ligand and forms **XV** (H= -36.3 kcal/mol). This event is followed by the second bridge forming using the water on In_A (**XVI**; H= -46.5 kcal/mol). Exogenous formate deprotonates the bridging water to form the hydroxyl bridge of **VIII**, which is the intermediate where pathways 1 and 2 converge.
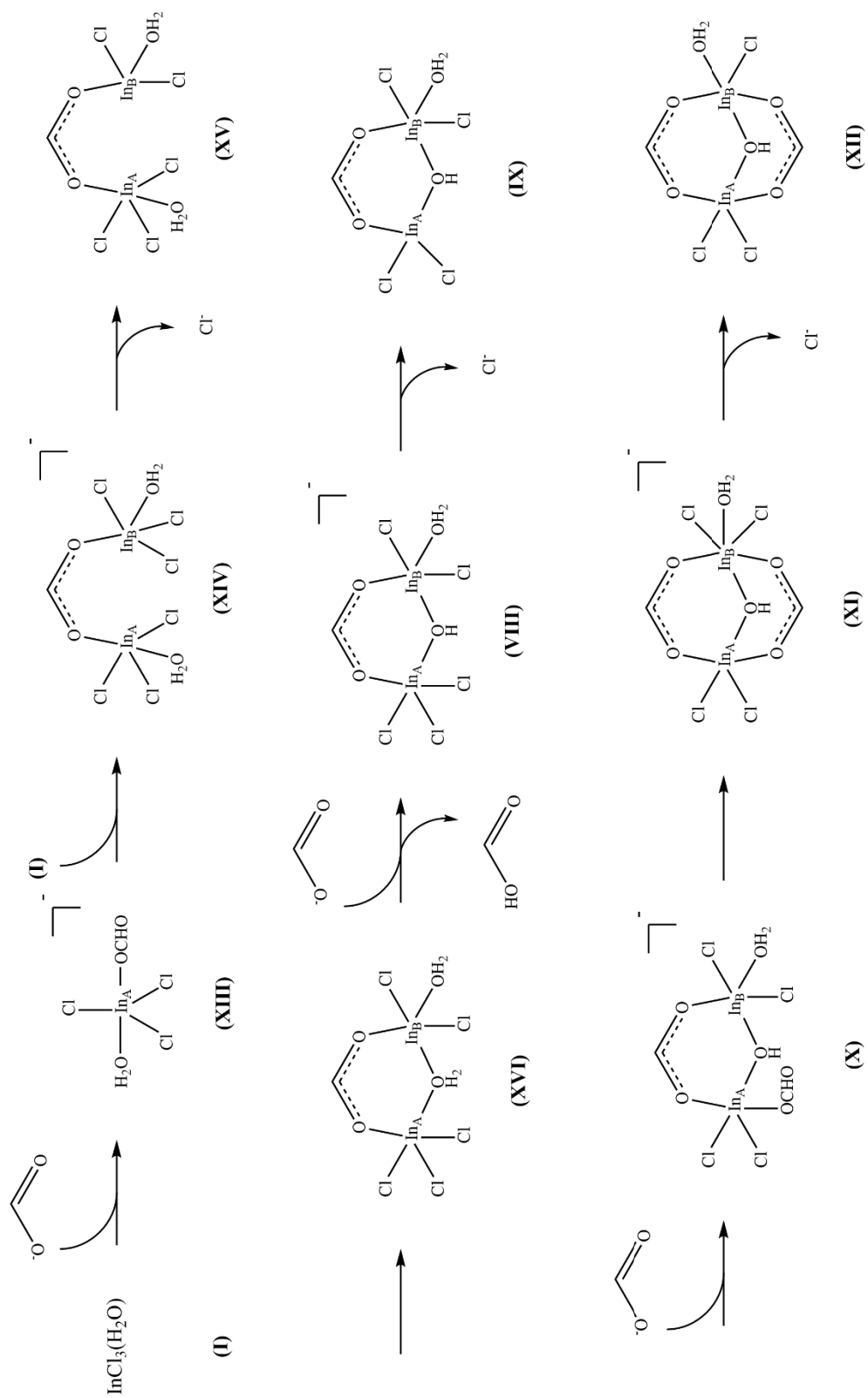
Scheme 8. The proposed mechanism of formation for **XII** as suggested by motif 2 of the unsolvated InCl$_3$(H$_2$O) system.
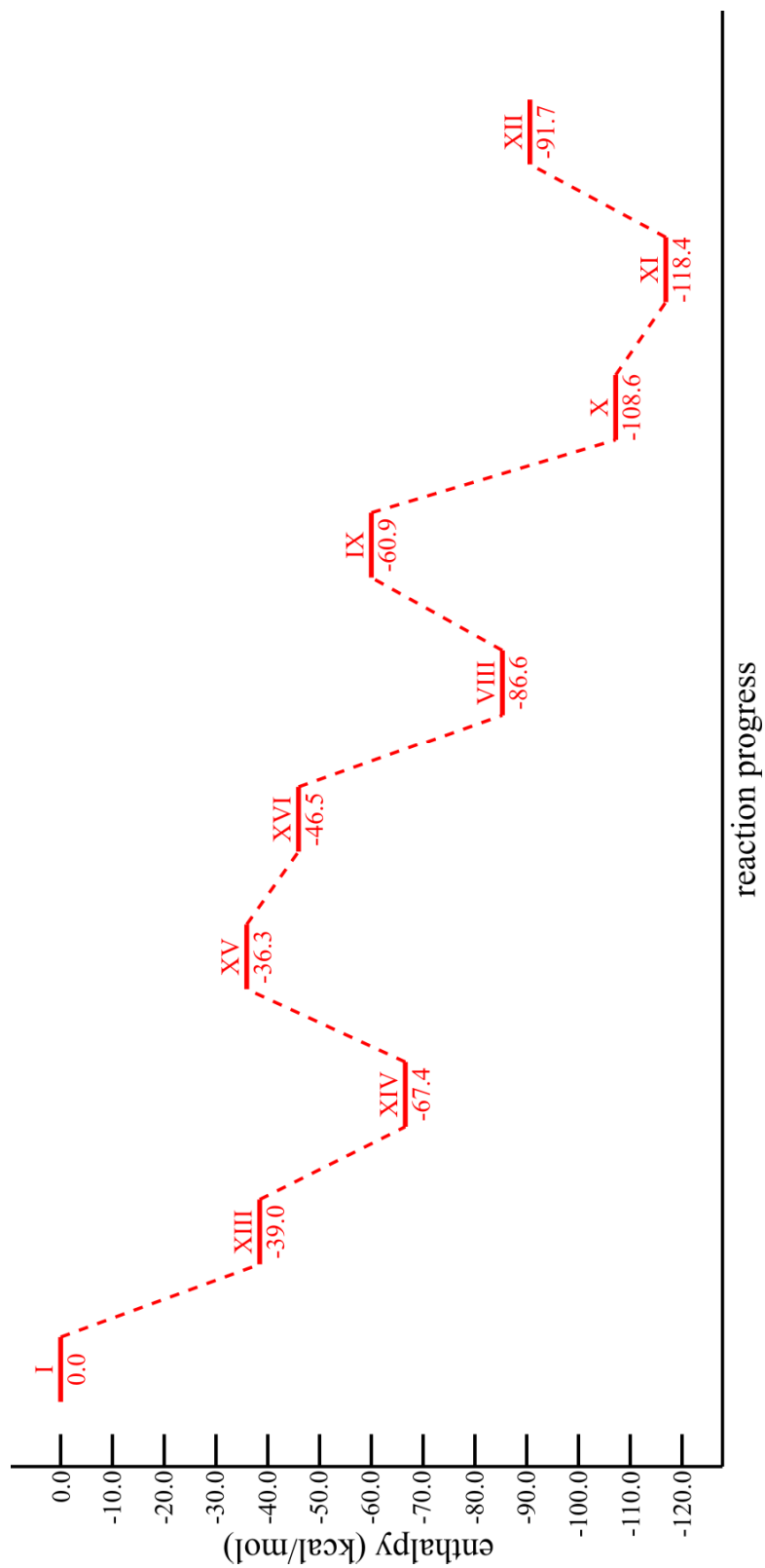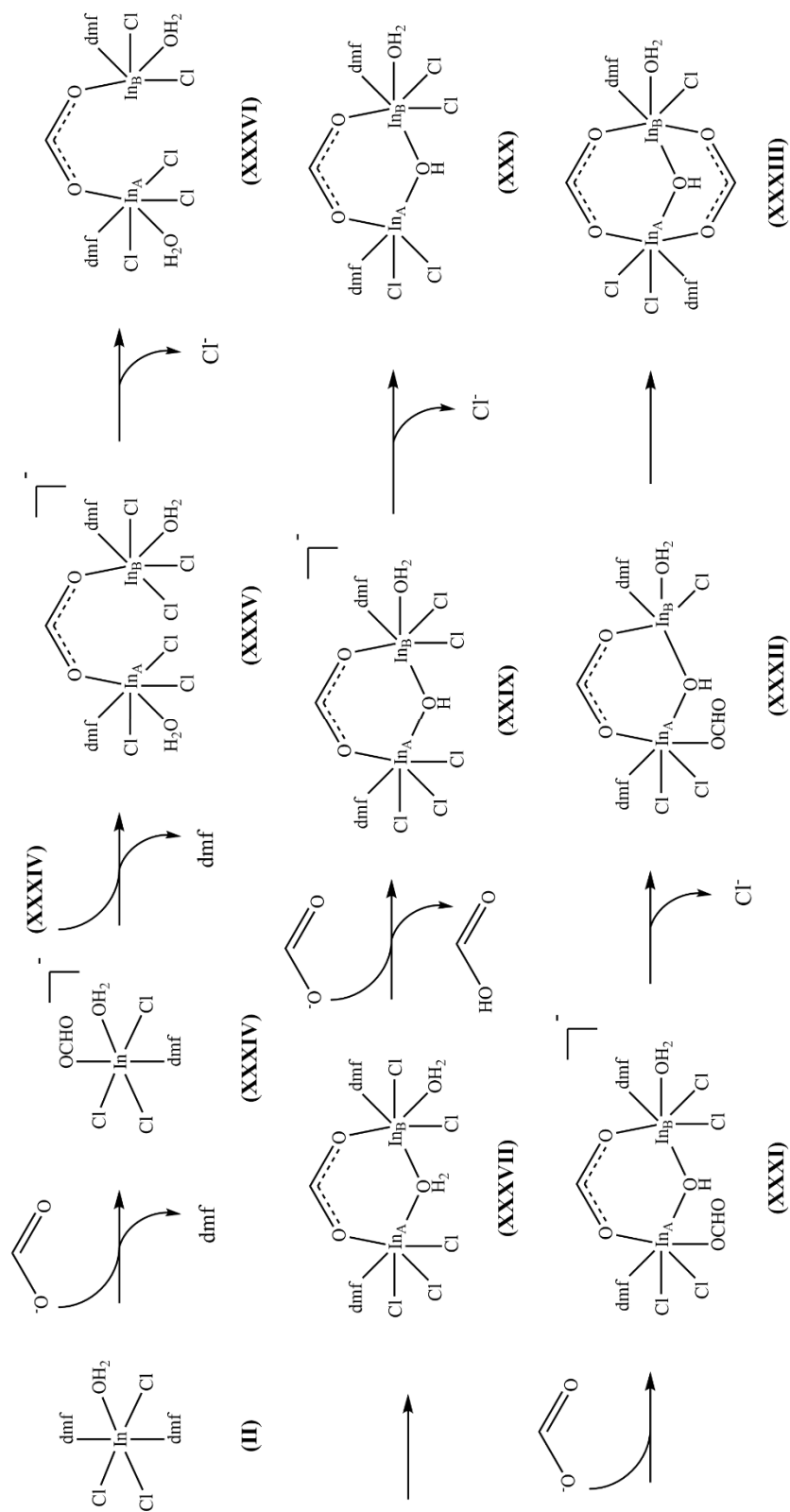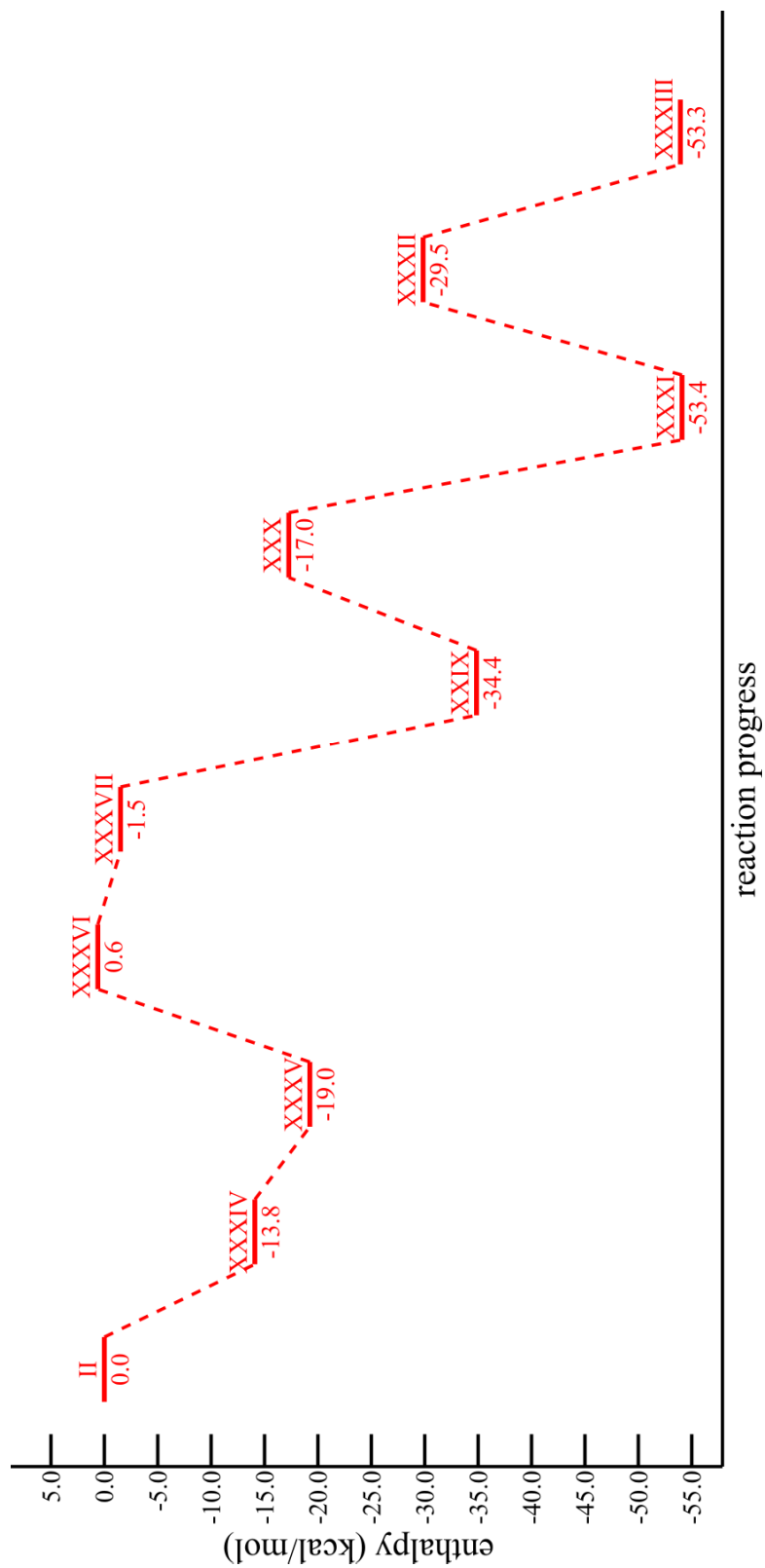
Figure 5. The energy profile diagram for pathway 2 of the unsolvated $InCl_3(H_2O)$ system plotted as reaction progress (X-axis) versus the relative enthalpy of formation (Y-axis).

Pathway 3a

Mechanism 3a begins the same as mechanism 2; however, all of the starting material is converted to **XIII** instead of only a single molecule of **I**. One of the two molecules of In-monocarboxylate sheds a chloride ligand—this molecule becomes the source of In_B (**XVII**; H= kcal/mol). In_B reacts with formate on the first equivalent of In-monocarboxylate which forms the first carboxylate bridged product, **XVIII** (H= -81.9 kcal/mol). A chloride ligand is shed from In_A, thus forming **XIX** (H= -50.9). The second bridge is then made at this step when the κ^1 formate bridges both In-atoms, making a symmetrical molecule (**XX**; H= -67.1 kcal/mol). The water on either In_A or In_B can then bridge both In-atoms to form **XXI** (H= -80.6 kcal/mol). Exogenous formate will deprotonate the μ^2 water which forms the lowest enthalpic molecule, **XI** (H= -118.4 kcal/mol); at this point, mechanism 3a converges with pathway 1 and 2.

Pathway 3b

For the final proposal, the unsolvated dimer mechanism follows the same scheme as mechanism 3a until intermediate **XIX** is produced. Rather than form a second bridge using the carboxylate, water on In_B connects both In-atoms. This step forms intermediate **XXII** (H= -45.8). The proceeding deprotonation of the μ^2 water produces intermediate **X**. This is where the pathway converges with mechanisms 1 and 2.
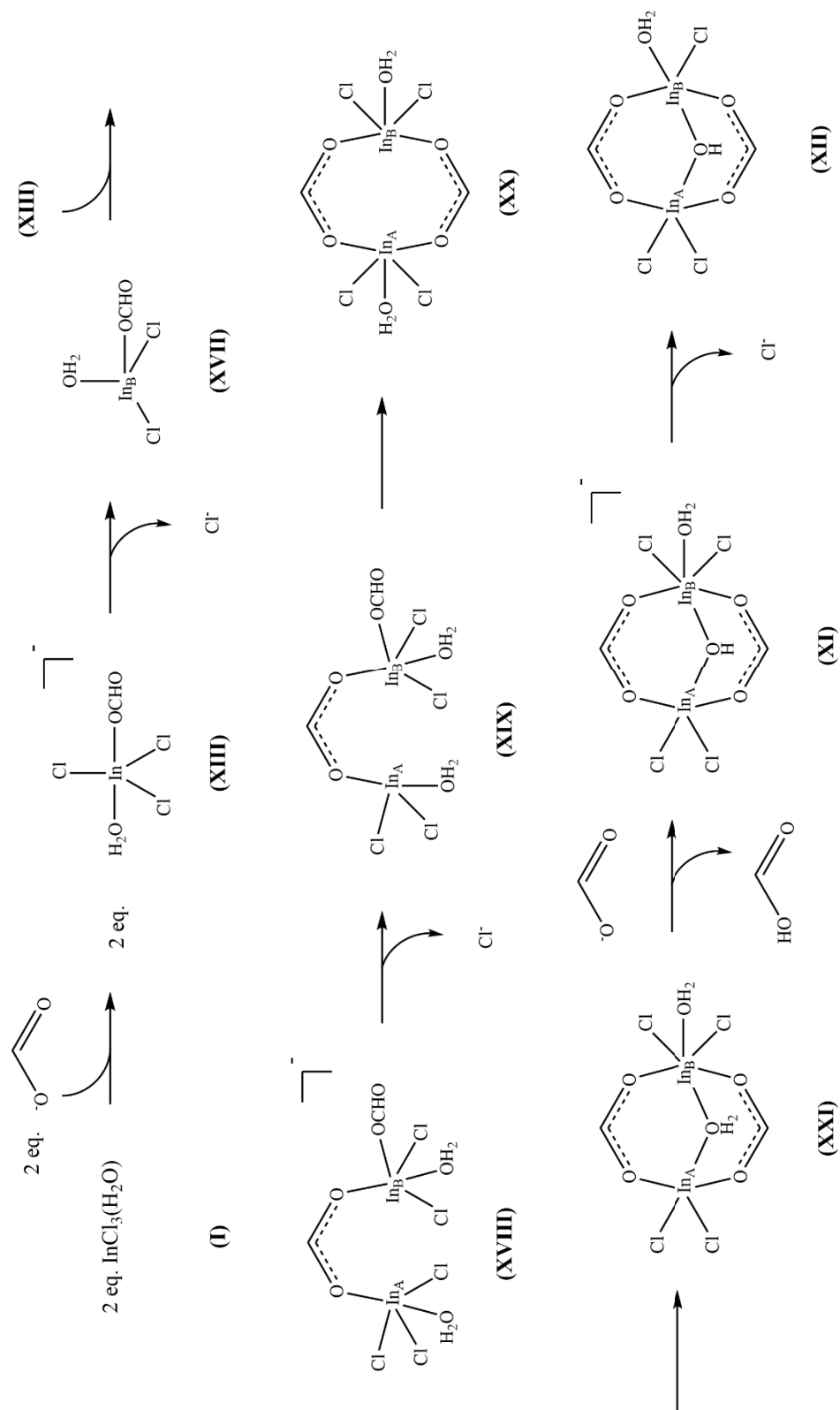
Scheme 9. The proposed mechanism of formation for **XII** as suggested by motif 3a of the unsolvated InCl$_3$(H$_2$O) system.
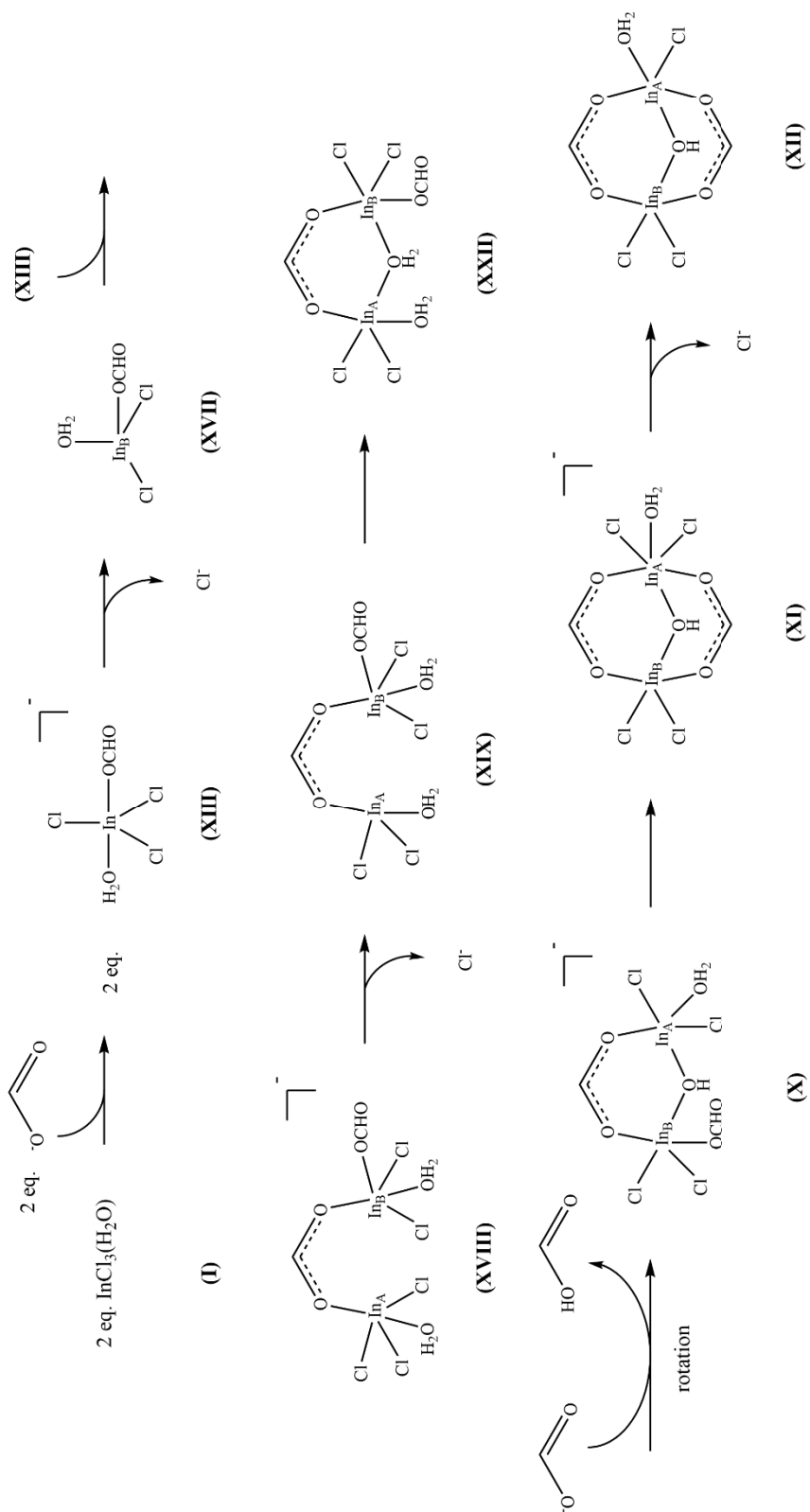
Scheme 10. The proposed mechanism of formation for **XII** as suggested by motif 3b of the unsolvated InCl₃(H₂O) system.
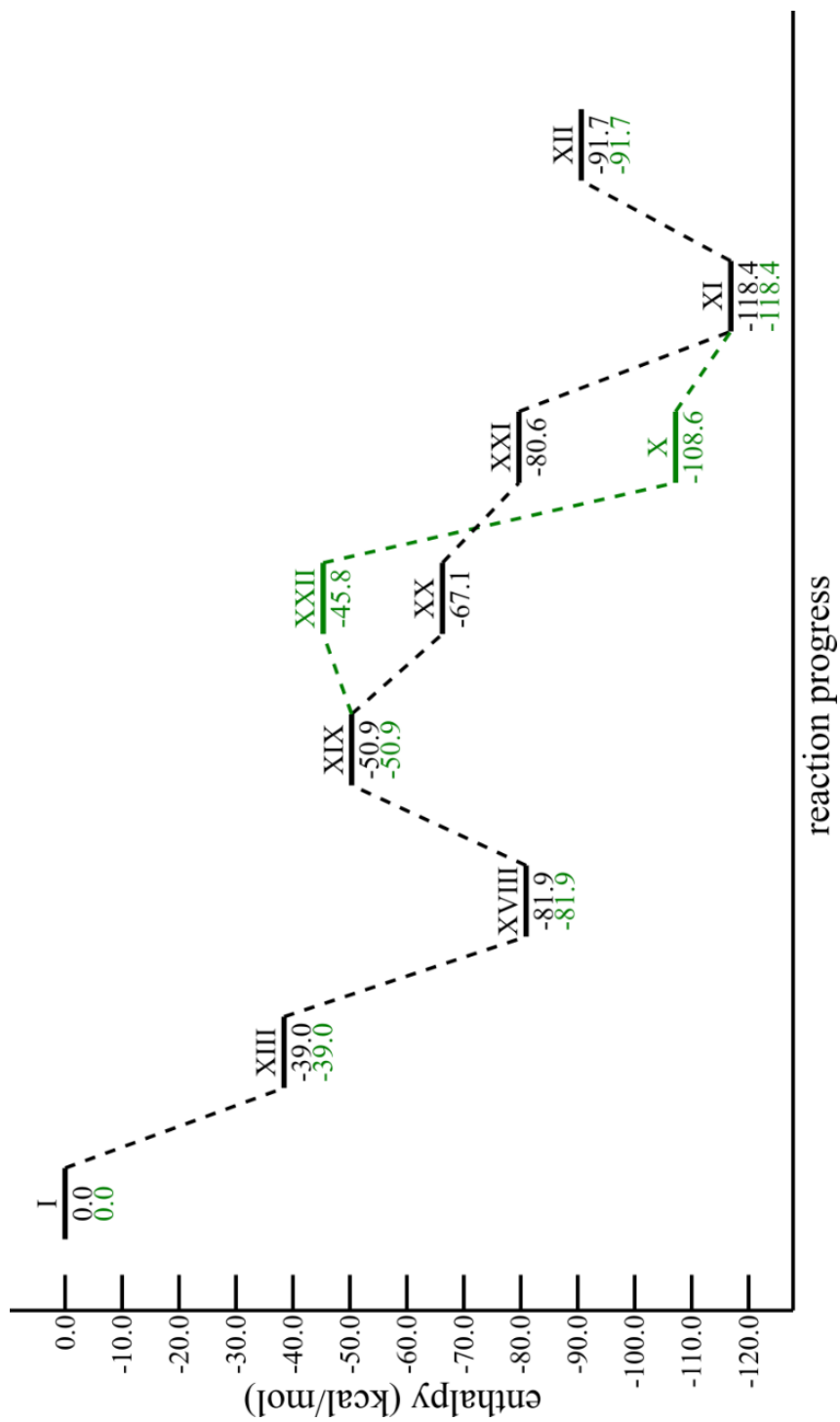
Figure 6. The energy profile diagram for pathway 3a (black) and 3b (green) of the unsolvated $InCl_3(H_2O)$ system plotted as reaction progress (X-axis) versus the relative enthalpy of formation (Y-axis).
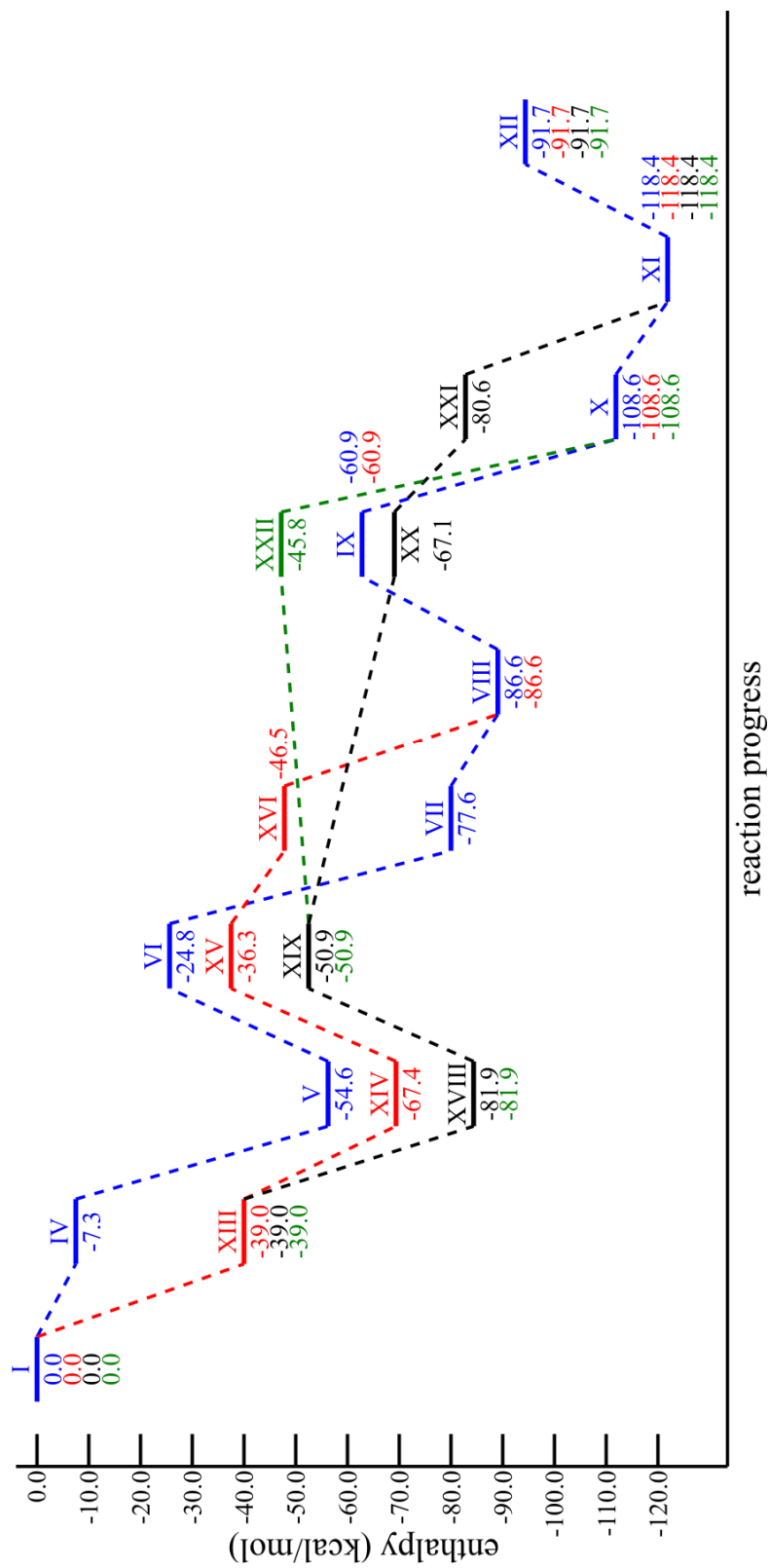
Figure 7. A stacked energy profile diagram of pathway 1-3b for the unsolvated InCl$_3$(H$_2$O) system. Blue : pathway 1; red : pathway 2; black : pathway 3a; green : pathway 3b.

Solvated InCl₃(H₂O) System

Pathway 1

The first proposed mechanism for the solvated $InCl_3(H_2O)$ system begins with one molecule of **II** shedding a DMF ligand (**XXIII**; H= 20.3 kcal/mol). **XXIII** will react with another equivalent of **II** and dimerize via bound water (**XXIV**; H= 10.2 kcal/mol). In this mechanism, the In-atom "donating" water is denoted as In_A, and the In-atom "accepting" water is denoted In_B. **XXIV** is then deprotonated by exogenous formate and forms **XXV** (H= -21.3 kcal/mol). **XXV** then proceeds to shed a DMF ligand from In_A which forms **XXVI** (H= -2.8 kcal/mol). Free formate then reoccupies the open coordination site (**XXVII**; H= -37.6 kcal/mol). Next, **XXVII** sheds a chloride ligand from In_B to create **XXVIII** (H= -21.3 kcal/mol). **XXIX** is made when both In-atoms are bridged using the κ^1 formate on In_A (H= -34.4 kcal/mol). A chloride ligand is then shed from In_A and makes **XXX** (H= -17.0 kcal/mol). Another equivalent of free formate then binds to In_A (**XXXI**; H= -53.4 kcal/mol). A final chloride ligand is shed from In_B (**XXXII**; H= -29.5 kcal/mol). This loss allows both In-atoms to be bridged by the κ^1 formate on In_A, and produces the proposed solvated dimer (**XXXIII**; -53.3 kcal/mol).
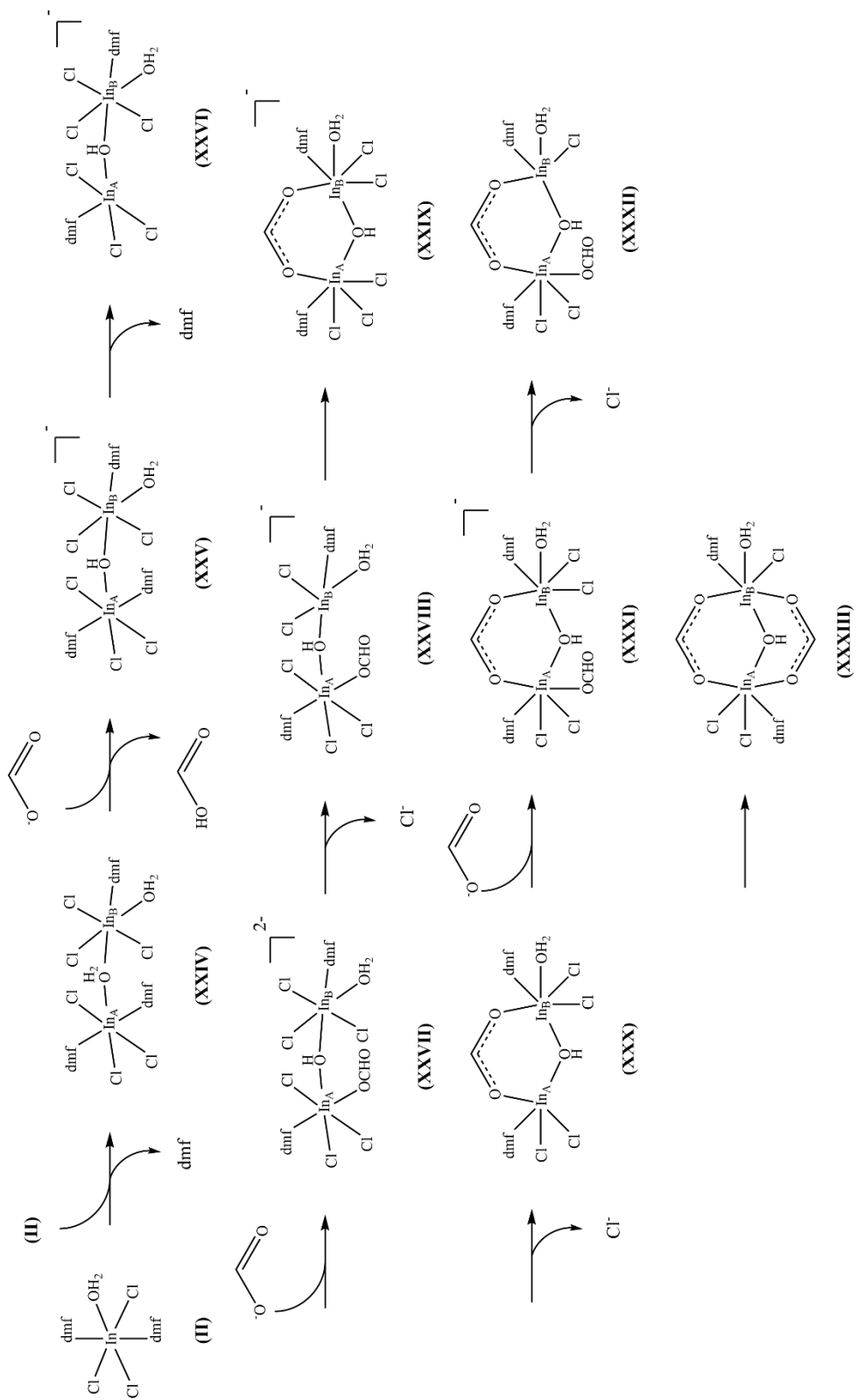
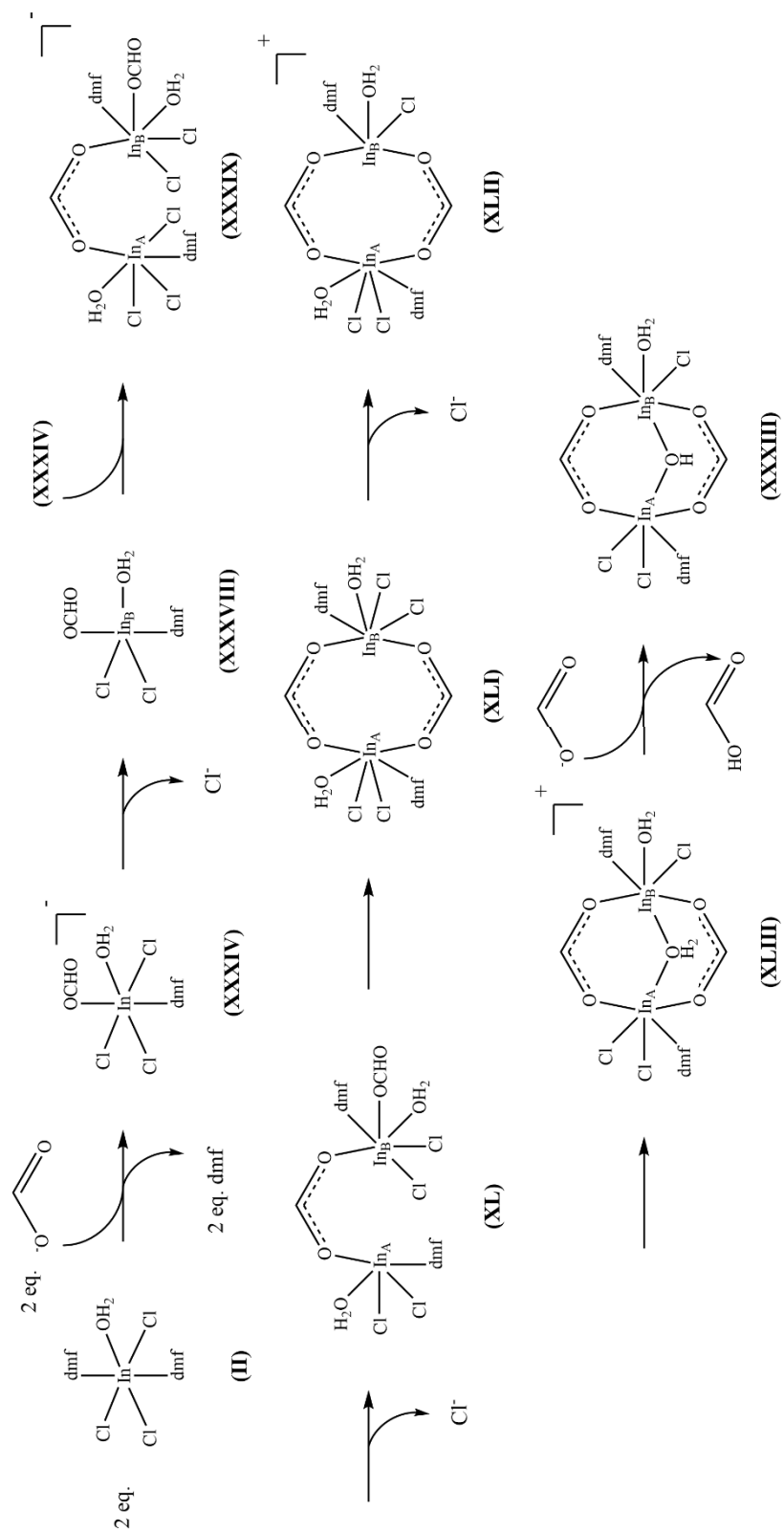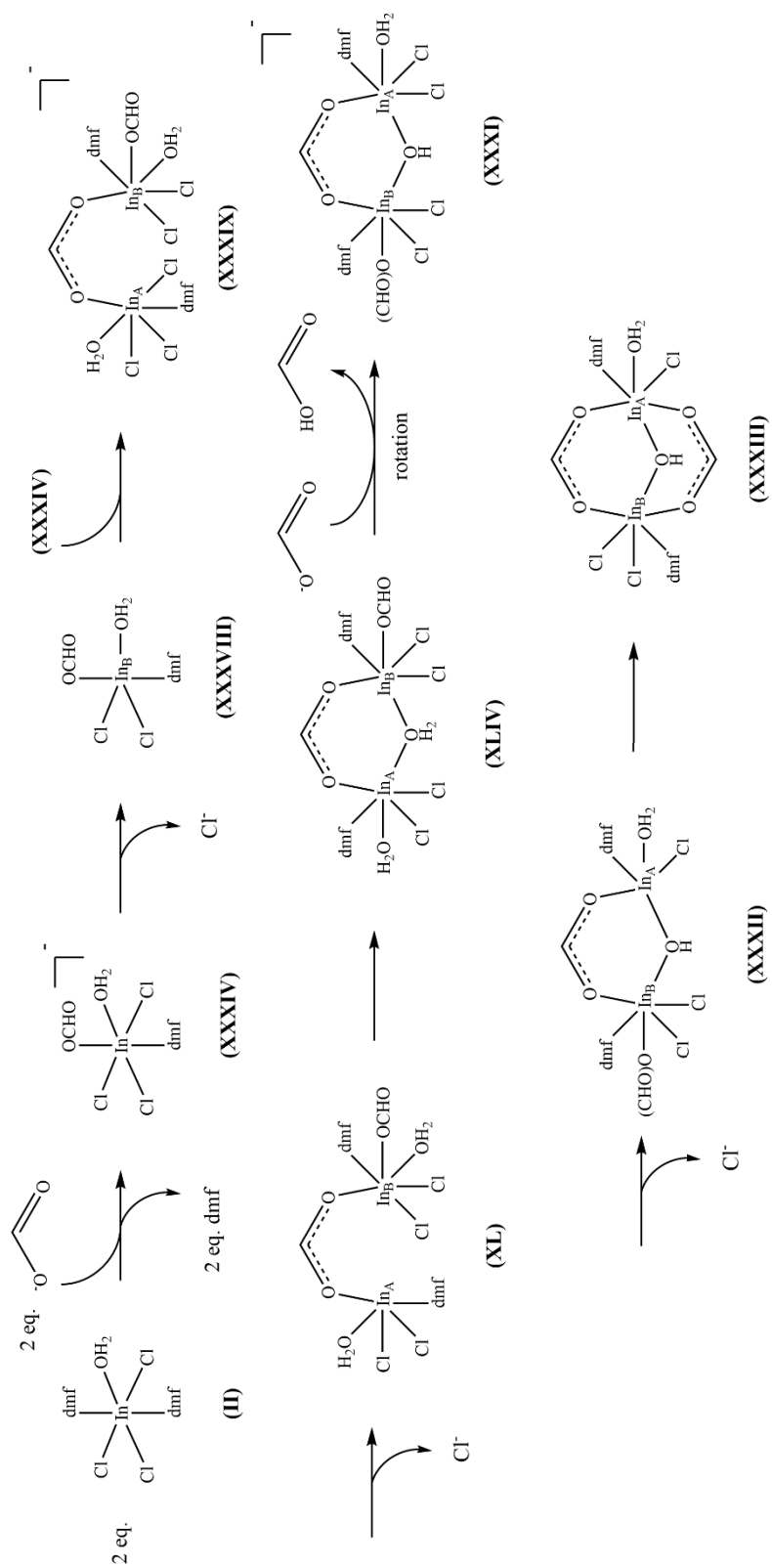**Scheme 11**. The proposed mechanism of formation for **XXXIII** as suggested by motif 1 of the solvated InCl$_3$(H$_2$O) system.
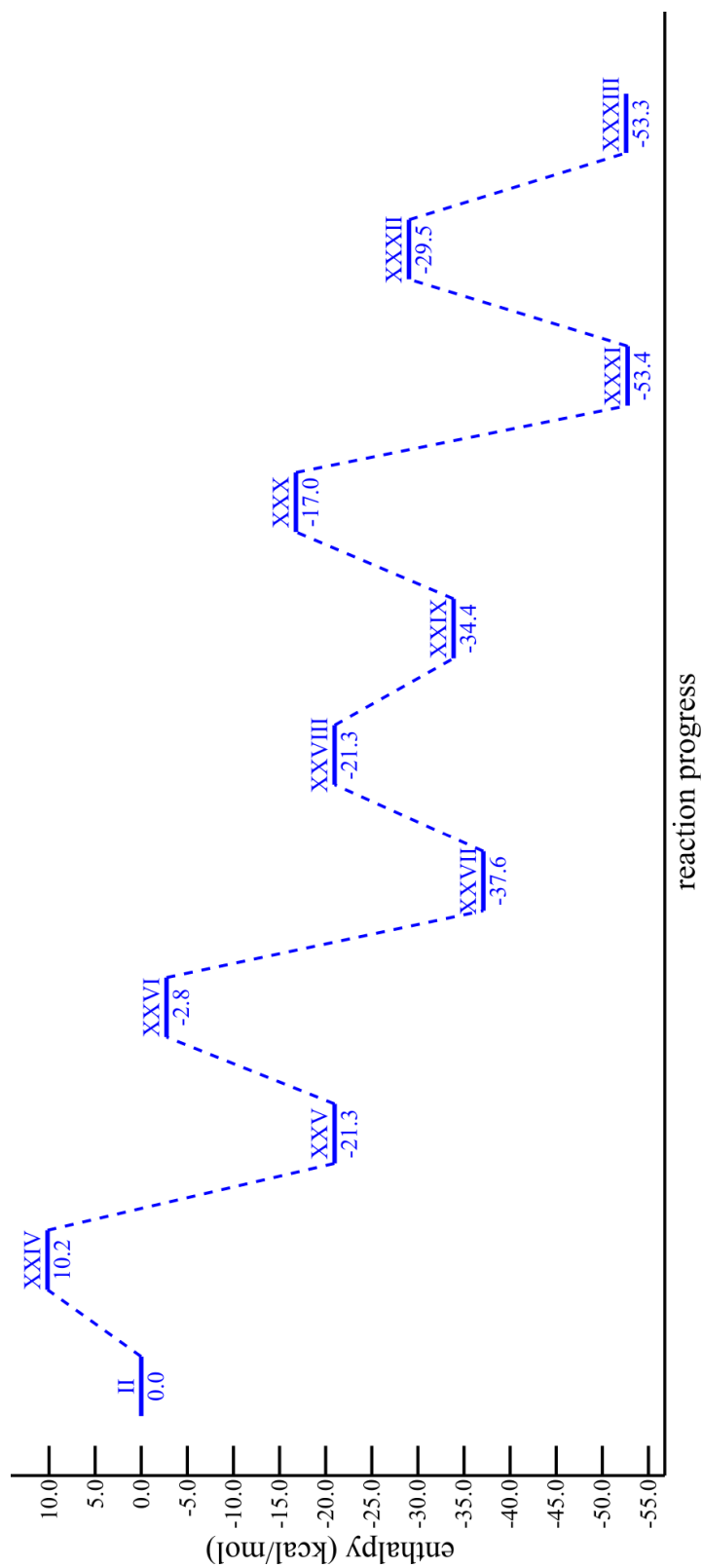
Figure 8. The energy profile diagram for pathway 1 of the solvated $InCl_3(H_2O)$ system plotted as reaction progress (X-axis) versus the relative enthalpy of formation (Y-axis).

28

Pathway 2

Pathway 2 begins by producing one equivalent of In-monocarboxylate. Initially, **II** has to first shed a ligand (**XXIII**; H= 20.3 kcal/mol). Free formate reoccupies the open coordination site and creates **XXXIV** (H= -13.8 kcal/mol). A second equivalent of **II** then sheds a DMF ligand. The In-atom "donating" the κ^1 formate will be referred to In$_A$, and the In-atom "accepting" the formate will be referred to In$_B$. **XXXIV** reacts with **XXIII** to form the carboxylate bridge of **XXXV** (H= -19.0 kcal/mol). A chloride ligand is then shed from In$_B$ which forms **XXXVI** (H= 0.6 kcal/mol). Water bound to In$_A$ is used to bridge both In-atoms (**XXXVII**; H= -1.5 kcal/mol). Exogenous formate is used to deprotonate the μ^2 water bridge and creates **XXIX**. This is the intermediate on which pathways 1 and 2 converge.

Scheme 12. The proposed mechanism of formation for **XXXIII** as suggested by motif 2 of the solvated InCl₃(H₂O) system.

Figure 9. The energy profile diagram for pathway 2 of the solvated $InCl_3(H_2O)$ system plotted as reaction progress (X-axis) versus the relative enthalpy of formation (Y-axis).

Pathway 3a

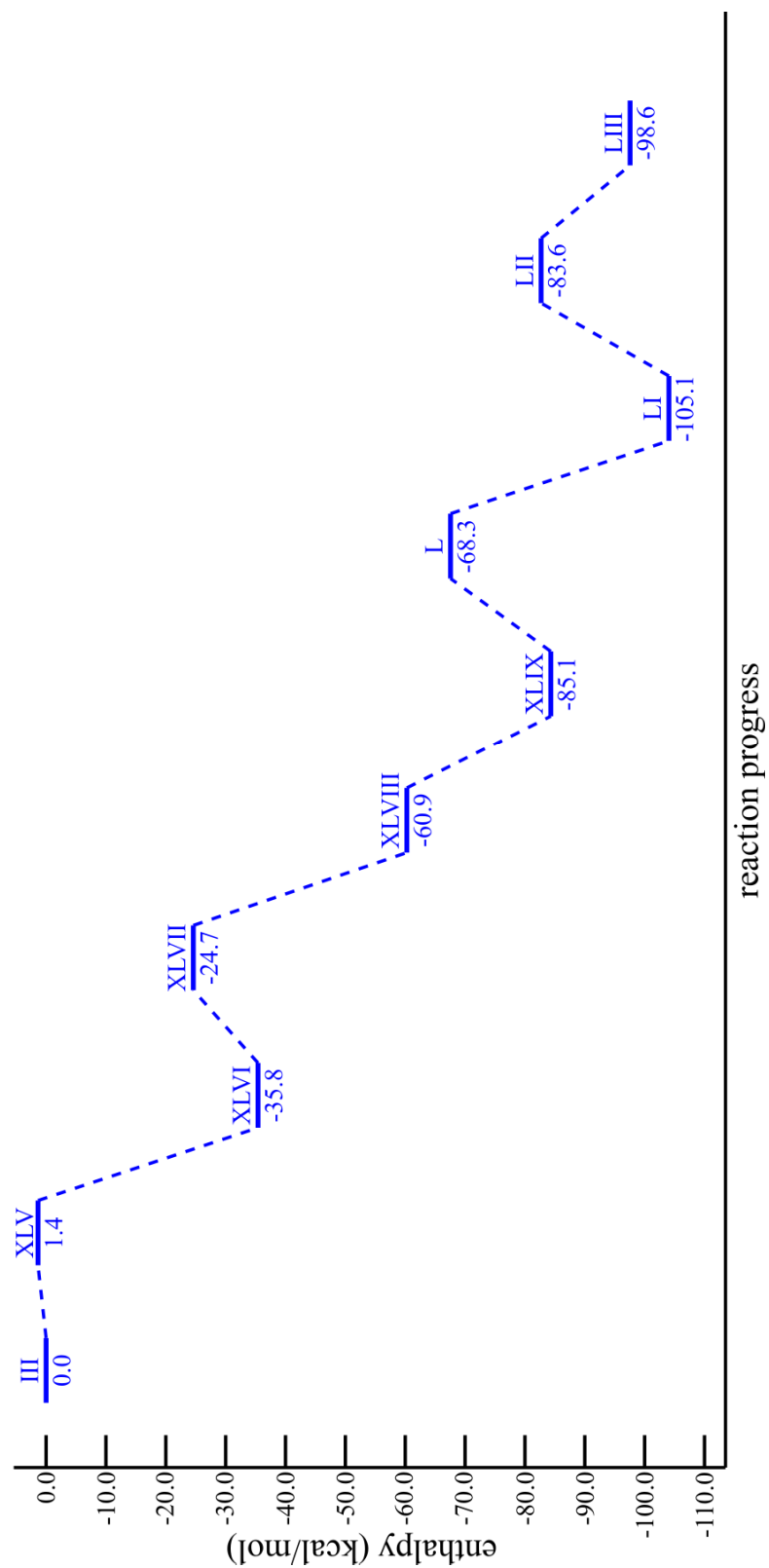Mechanism 3a begins the same as mechanism 2; however, all of the starting material is converted to **XXXIV** instead. One of the two molecules of In-monocarboxylate then sheds a chloride ligand (**XXXVIII**; H= 4.8 kcal/mol). Reacting the remaining molecule of **XXXIV** with **XXXVII** creates **XXXIX** (H= -38.6 kcal/mol); the In-atom "donating" the formate will be the source of In_A, and the In-atom "accepting" the formate will be the source of In_B. In_A sheds a chloride ligand producing **XL** (H= -16.8 kcal/mol). The κ^1 formate on In_B then bridges both In-atoms (**XLI**; H= -30.5 kcal/mol). A chloride ligand is shed from In_B, which opens a coordination site (**XLII**; H= -11.2 kcal/mol). Water from In_A reoccupies the site by bridging both In-atoms (**XLIII**; H= -16.3 kcal/mol). Finally, **XLIII** is deprotonated by exogenous formate to produce the proposed solvated dimer, **XXXIII**.

Pathway 3b

Mechanism 3b is derived from solvated mechanism 3a and begins by creating the same equivalents of In-monocarboxylate. The pathway will follow the same mechanism until **XL** is made. Once formed, water on In_B bridges both In-atoms (**XLIV**; H= -17.7 kcal/mol). Exogenous formate will deprotonate the bridging water, which makes **XXXI**. This is where the pathway converges with mechanisms 1 and 2.

Scheme 13. The proposed mechanism of formation for **XXXIII** as suggested by motif 3a of the solvated InCl$_3$(H$_2$O) system.

Scheme 14. The proposed mechanism of formation for **XXXIII** as suggested by motif 3b of the solvated InCl₃(H₂O) system.
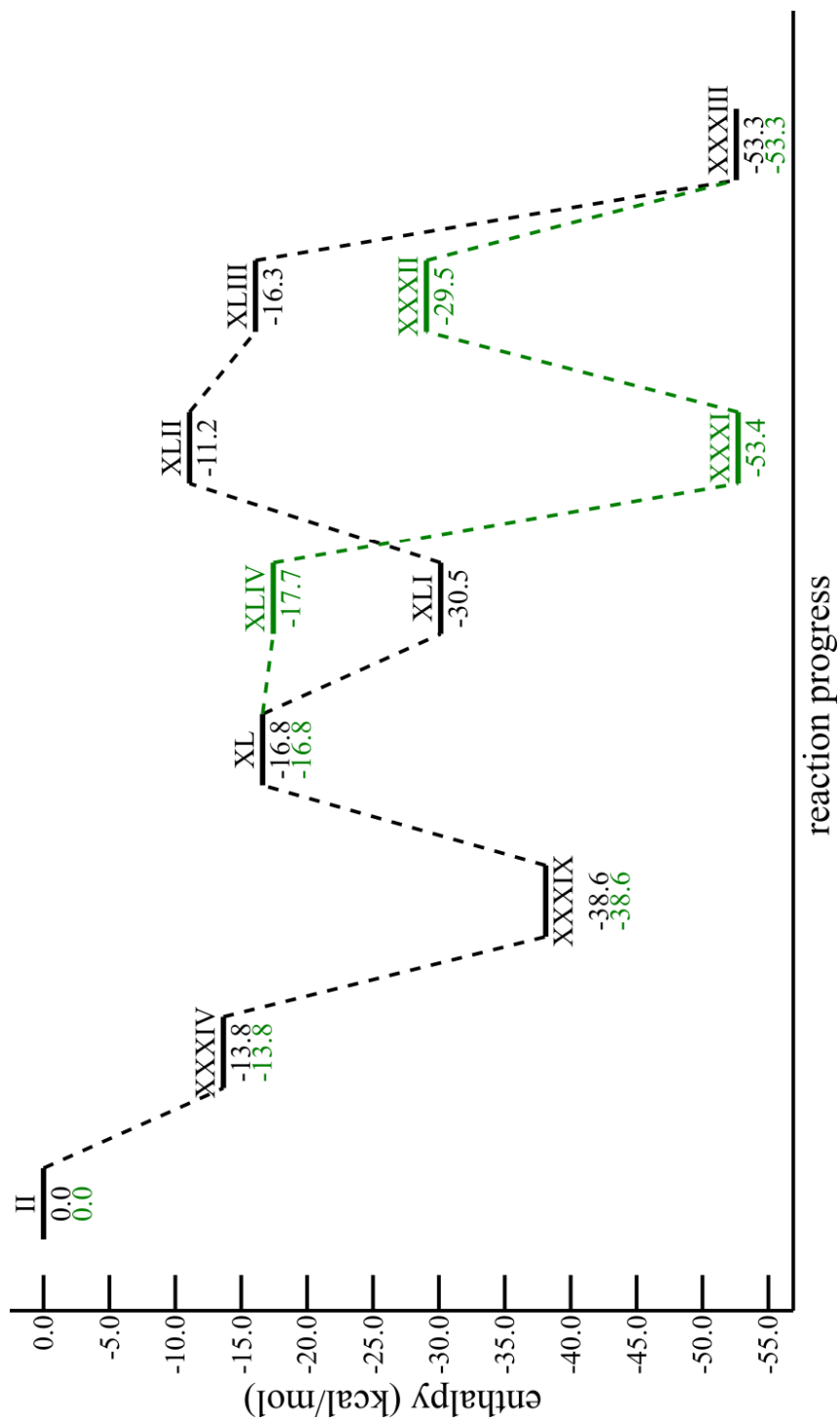
Figure 10. The energy profile diagram for pathway 3a (black) and 3b (green) of the solvated $InCl_3(H_2O)$ system plotted as reaction progress (X-axis) versus the relative enthalpy of formation (Y-axis).
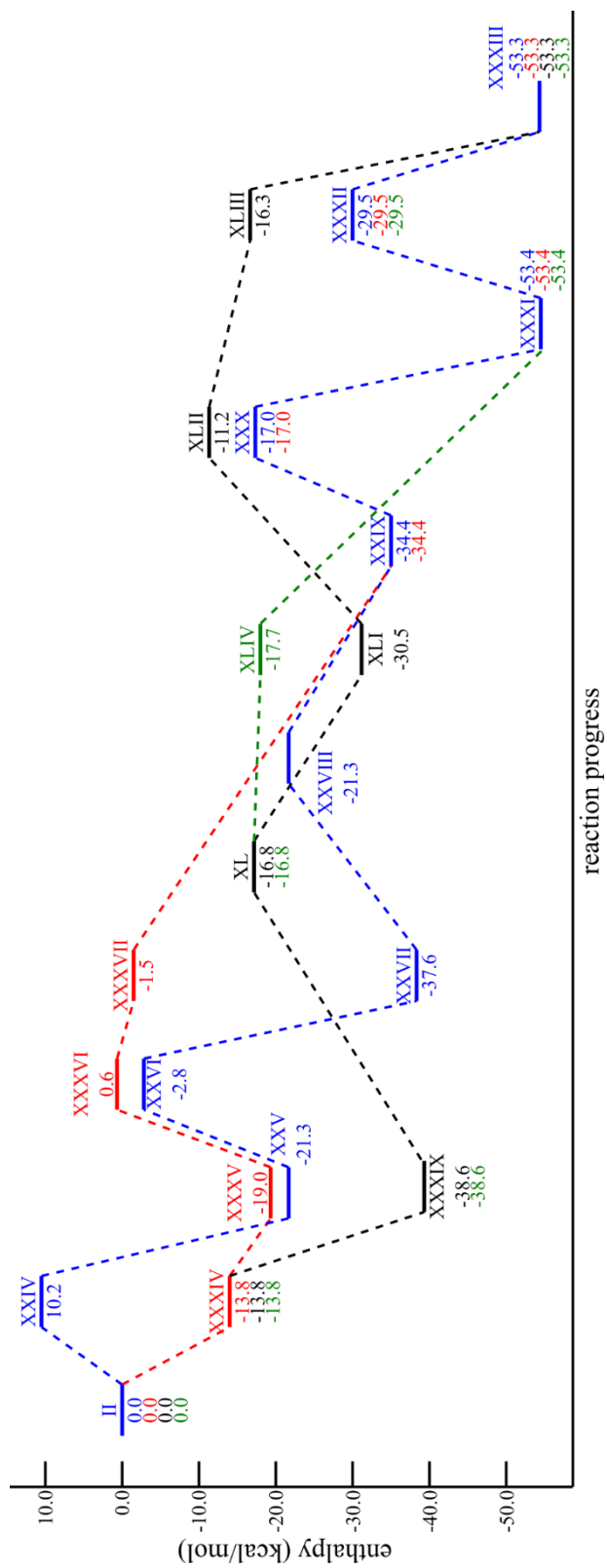
Figure 11. A stacked energy profile diagram of pathway 1-3b for the solvated InCl₃(H₂O) system. Blue : pathway 1; red : pathway 2; black : pathway 3a; green : pathway 3b.

Solvated In(NO₃)₃(H₂O) System

Pathway 1

Pathway 1 begins with two equivalents of **III** dimerizing via the water on either molecule (**XLV**; H= 1.4 kcal/mol). The In-atom "donating" the water will be the source of In$_A$, and the In-atom "accepting" the water will be the source of In$_B$. The μ^2 water bridge is deprotonated by exogenous formate (**XLVI**; H= -35.8 kcal/mol). Next, a DMF ligand is shed from In$_B$ (**XLVII**; H= -24.7). In$_B$ then binds to free formate (**XLVIII**; H= -60.9 kcal/mol). The κ^1 formate on In$_B$ bridges both In-atoms, which makes **XLIX** (H= -85.1 kcal/mol). A DMF ligand can then be shed from In$_A$ so **L** can be formed (H= -68.3 kcal/mol). Another equivalent of formate binds to In$_A$ and **LI** is produced (H= -105.1 kcal/mol). DMF is then shed, and intermediate **LII** is made (H= -83.6 kcal/mol). Finally, the κ^1 formate on In$_A$ bridges both In-atoms to form the proposed solvated dimer, **LIII** (H= -98.6 kcal/mol).

Scheme 15. The proposed mechanism of formation for **LIII** as suggested by motif 1 of the solvated In(NO₃)₃(H₂O) system.

Figure 12. The energy profile diagram for pathway 1 of the solvated $In(NO_3)_3(H_2O)$ system plotted as reaction progress (X-axis) versus the relative enthalpy of formation (Y-axis).

Pathway 2

Mechanism 2 begins with reacting one molecule of formate and one molecule of **III** (**LIV**; H= -43.1 kcal/mol). DMF is shed from this species and **LV** is formed (H= -22.2 kcal/mol). This molecule, **LV**, will react with another equivalent of **III** to produce **LVI** (H= -33.9 kcal/mol). The In-atom "donating" the carboxylate will be the source of In_A, and the In-atom "accepting" the carboxylate will be the source of In_B. DMF is then shed from In_B, making the symmetrical intermediate **LVII** (H= -10.3 kcal/mol). Subsequently, water bound to In_A reoccupies the coordination site by bridging both In-atoms (**LVIII**, H= -17.2 kcal/mol). Exogenous formate is used to deprotonate the bridging water, and the pathway then converges with mechanism 1 at intermediate **L**.
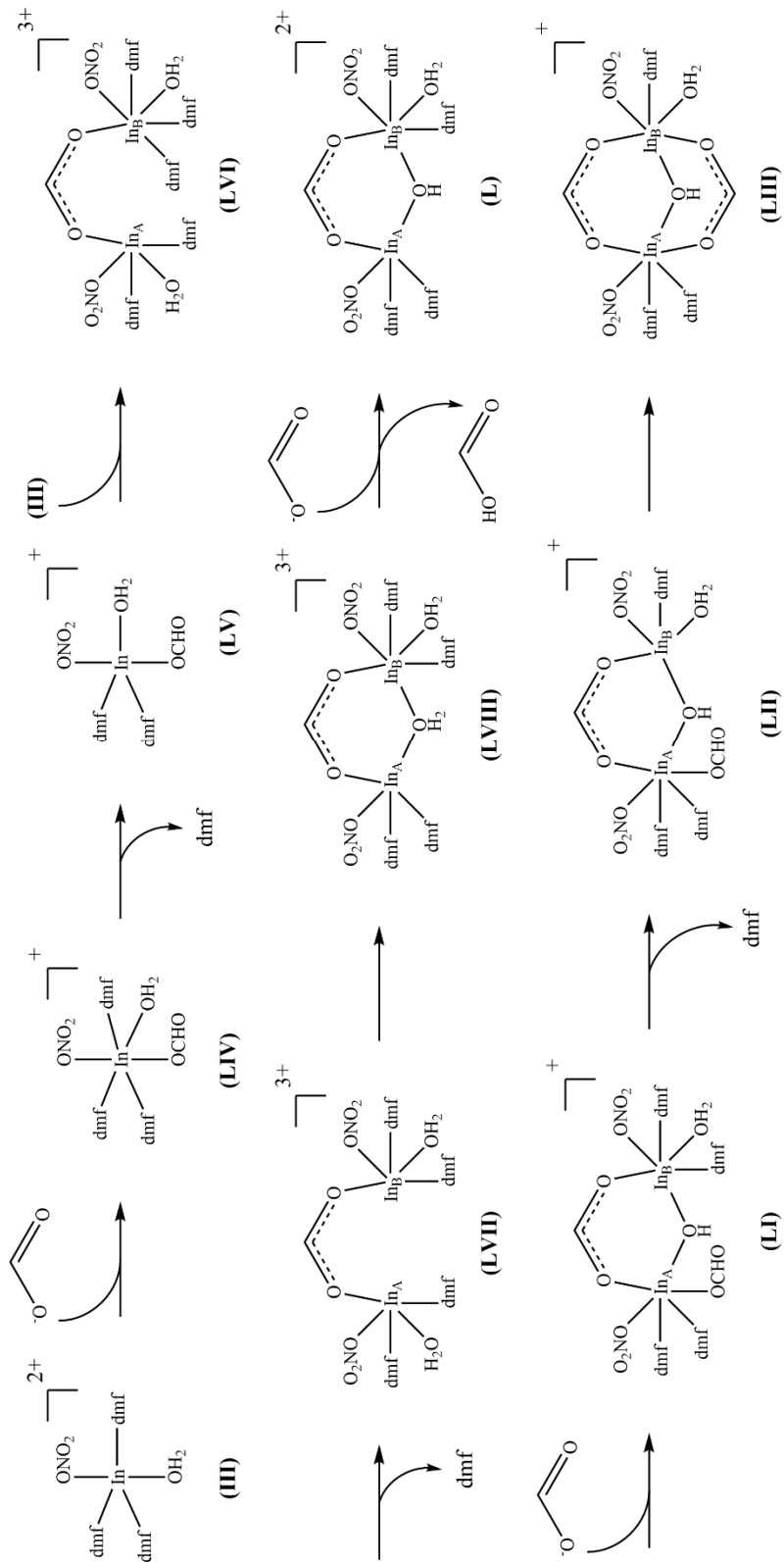
Scheme 16. The proposed mechanism of formation for **LIII** as suggested by motif 2 of the solvated In(NO₃)₃(H₂O) system.

41
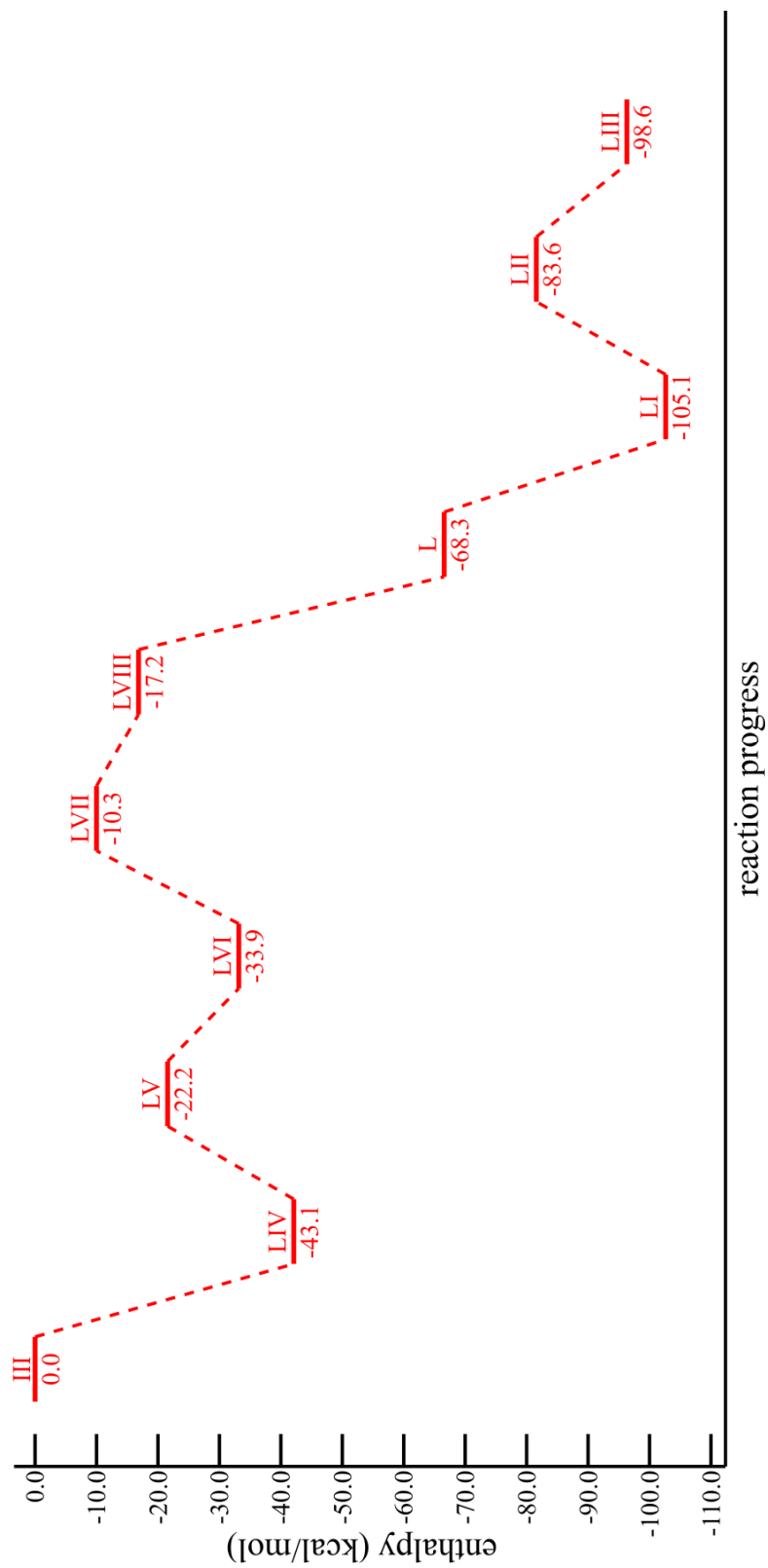
Figure 13. The energy profile diagram for pathway 2 of the solvated $In(NO_3)_3(H_2O)$ system plotted as reaction progress (X-axis) versus the relative enthalpy of formation (Y-axis).

Pathway 3a

Mechanism 3a converts all the starting material to **LV**. Next, one of the two molecules of In-monocarboxylate will use its formate to dimerize (**LIX**; H= -56.2 kcal/mol). The In-atom "donating" the formate will be the source of In_A, and the In-atom "accepting" the formate will be the source of In_B. The κ^1 formate on In_B then bridges both of the In-atoms to produce **LX** (H= -66.0 kcal/mol). Afterwards, In_B on **LX** sheds an equivalent of DMF (**LXI**; H= -40.8 kcal/mol). Using the water on In_A, both In-atoms are bridged for a third time (**LXII**; H= -64.5 kcal/mol). Finally, the deprotonation of the bridging water using exogenous formate produces the proposed dimer, **613** (H= -98.6 kcal/mol).

Pathway 3b

Mechanism 3b also converts all starting material to **LV** and follows the same mechanism seen previously until **LIX** is produced. Just as pathway 3a, the In-atom "donating" the formate will be the source of In_A and the In-atom "accepting" the formate will be the source of In_B. After the formation of **LIX**, water on In_B bridges both In-atoms and creates **LXIII** (H= -66.2 kcal/mol). Exogenous formate will deprotonate the μ^2 water which makes **LI**. This is where the pathway converges with mechanism 1 and 2.
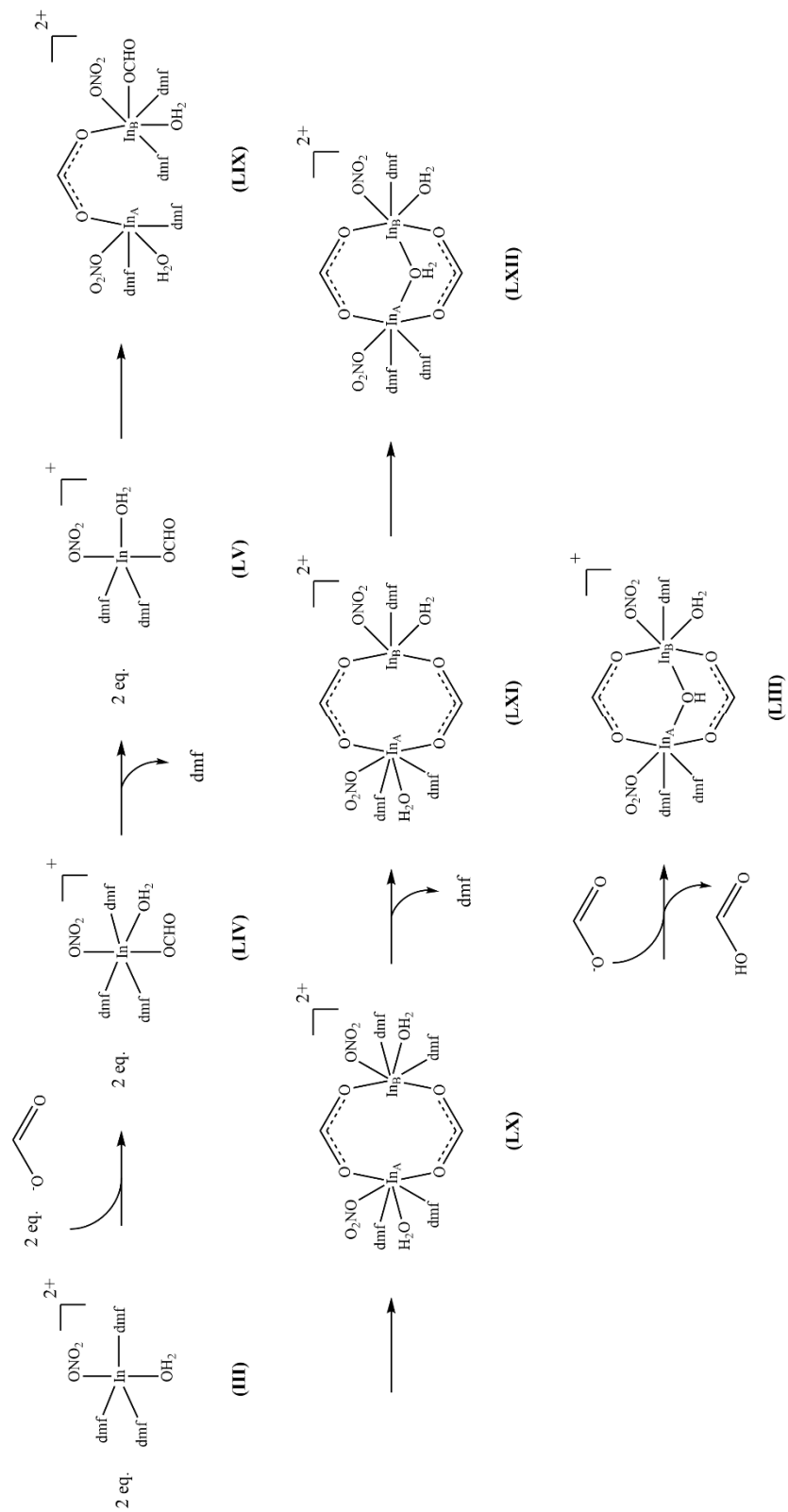
Scheme 17. The proposed mechanism of formation for **LIII** as suggested by motif 3a of the solvated In(NO₃)₃(H₂O) system.

44
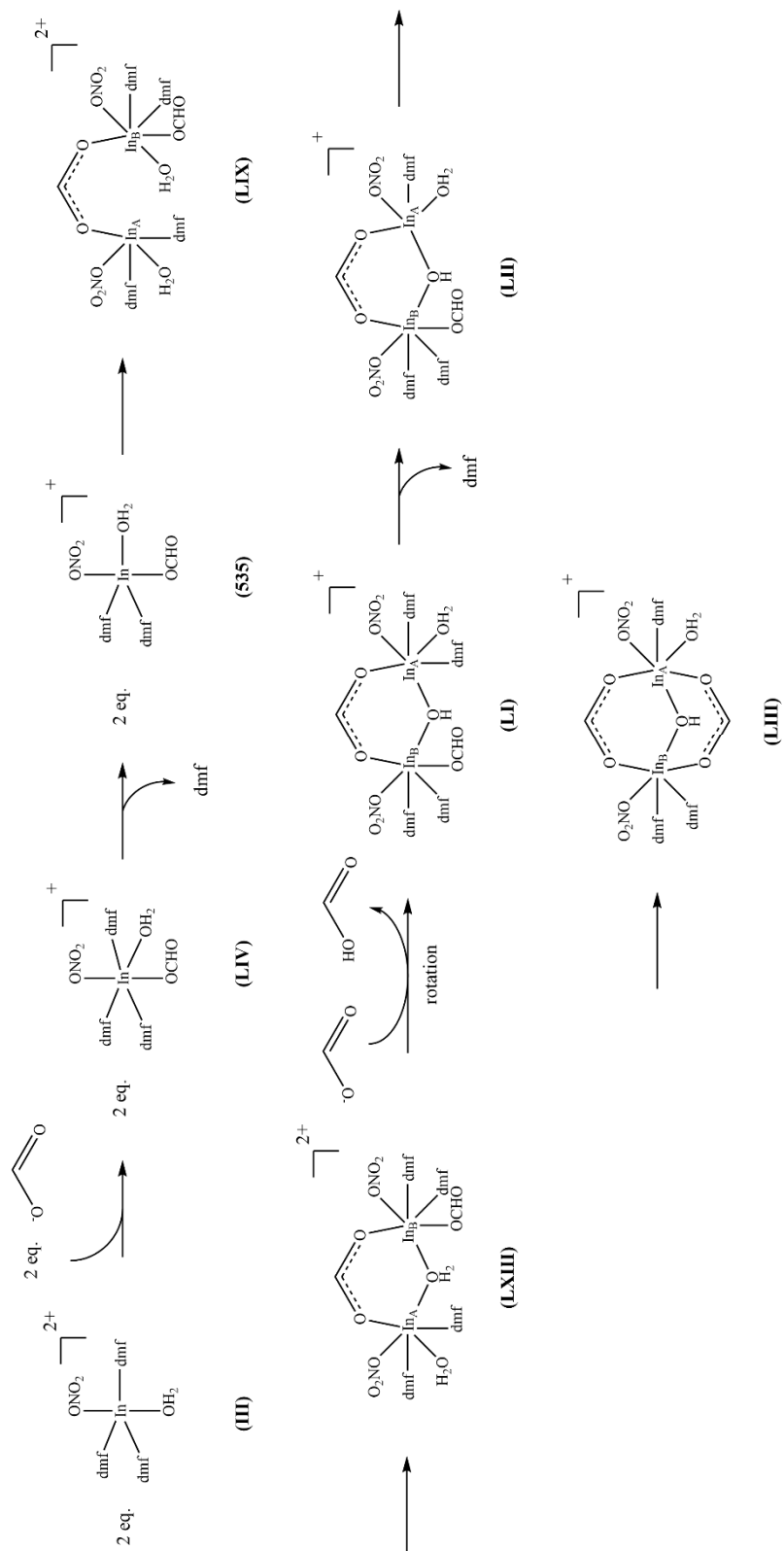
Scheme 18. The proposed mechanism of formation for **LIII** as suggested by motif 3b of the solvated In(NO₃)₃(H₂O) system.

45
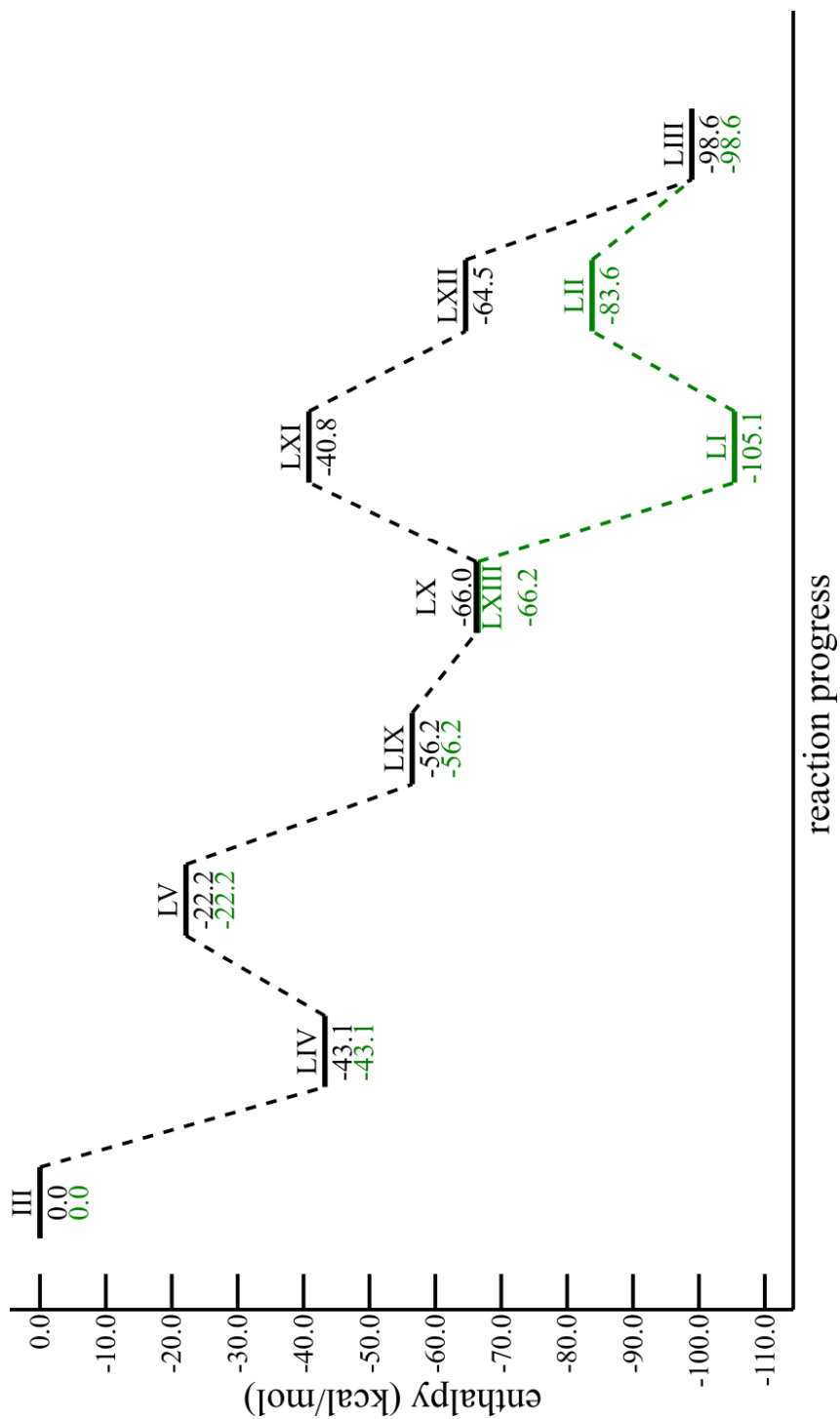
Figure 14. The energy profile diagram for pathway 3a (black) and 3b (green) of the solvated $In(NO_3)_3(H_2O)$ system plotted as reaction progress (X-axis) versus the relative enthalpy of formation (Y-axis).
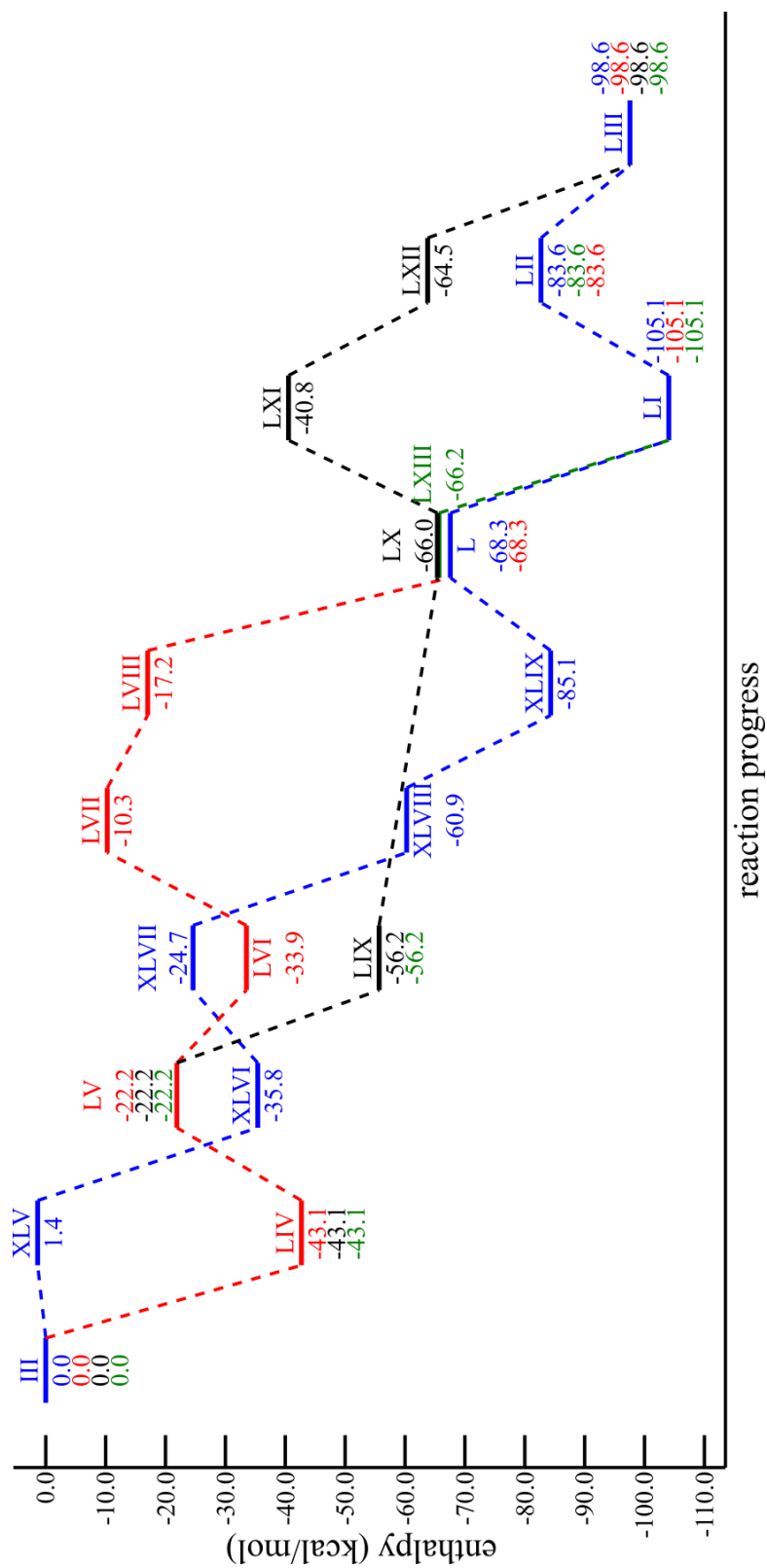
Figure 15. A stacked energy profile diagram of pathway 1-3b for the solvated In(NO$_3$)$_3$(H$_2$O) system. Blue : pathway 1; red : pathway 2; black : pathway 3a; green : pathway 3b.

III. Discussion

When comparing pathway 1 for both systems containing $InCl_3$ and the solvated $In(NO_3)_3$ system, it is appers that that the unsolvated $InCl_3(H_2O)$ system is the most enthalpically favored pathway; however, this is because the energy of the molecules calculated creates a higher starting point for the relative energies. What we can learn from this enthalpy diagram is that the source of indium prefers octahedral geometry over lower coordinated geometries. Looking at pathway 1 for the unsolvated $InCl_3(H_2O)$ system shows that intermediate **XI** has the lowest enthalpy at -118.4 kcal/mol. The molecular structure that belongs to this value contains the only octahedral In-atom in the proposed mechanism. In a relative comparison, the pathway for both solvated systems begin coordinatively saturated and return to an octahedral geometry at the end of their respective mechanisms. Conversely, the geometry for the unsolvated $InCl_3(H_2O)$ system begins tetrahedral (four-coordinated) and ends with both In-atoms of the dimer being trigonal bipyramidal (five-coordinated). Although each In-atom of end product **XII** has gained one occupied coordination site, the drastic enthalpy change shows how desirable it is for indium to achieve a degree of coordination, and is arguably the most useful information gained from those calculations. As a result, only the solvated systems were used for enthalpic and mechanistic comparisons because of their similar octahedral geometry.

Both solvated systems and all mechanism proposed herein contains several similar steps including water bridging and deprotonation, formate binding (either when an In-atom is monomeric or dimeric), both In-atoms bridging via formate, and some variation of ligand shedding. Deprotonation of water is systematically carried out by formate regardless of the system or pathway, and is originally proposed as occurring after the In-$(\mu\text{-}OH_2)$-In bonds

have been made. As an alternative to deprotonation of the water bridge after formation, the deprotonation of the μ^1 water on **II** and **III** before creating the hydroxyl bridge was examined and compared. For pathway 1 of the solvated $InCl_3(H_2O)$ system, deprotonation of the μ^1 water on **II** lowered the total relative enthalpy to -4.1 kcal/mol (**LXIV**). The loss of DMF on a second equivalent of **II** and the following bridging of In-atoms using the μ^1 hydroxyl on **LXIV** then creates the already proposed **XXV**.
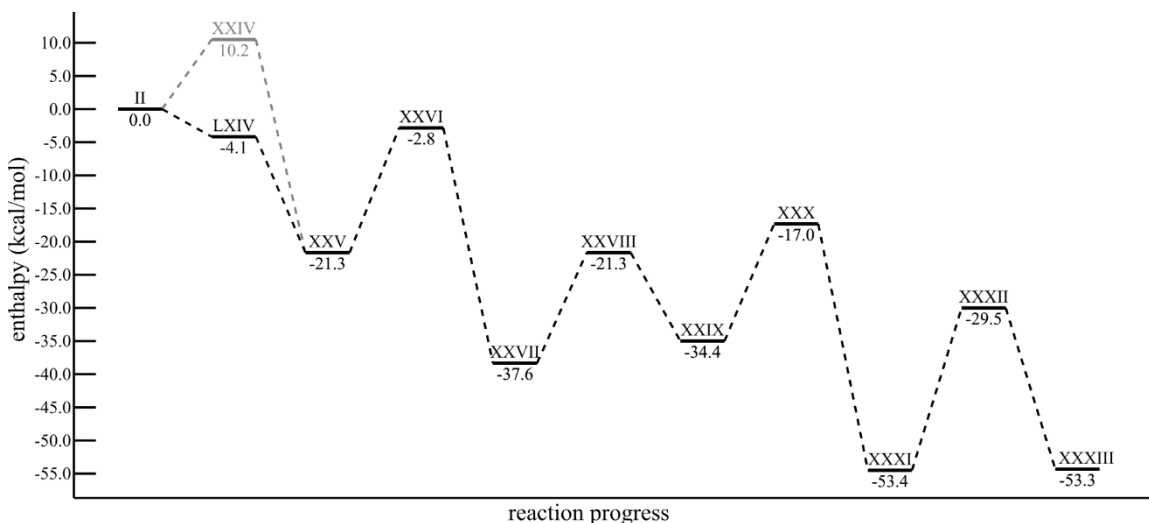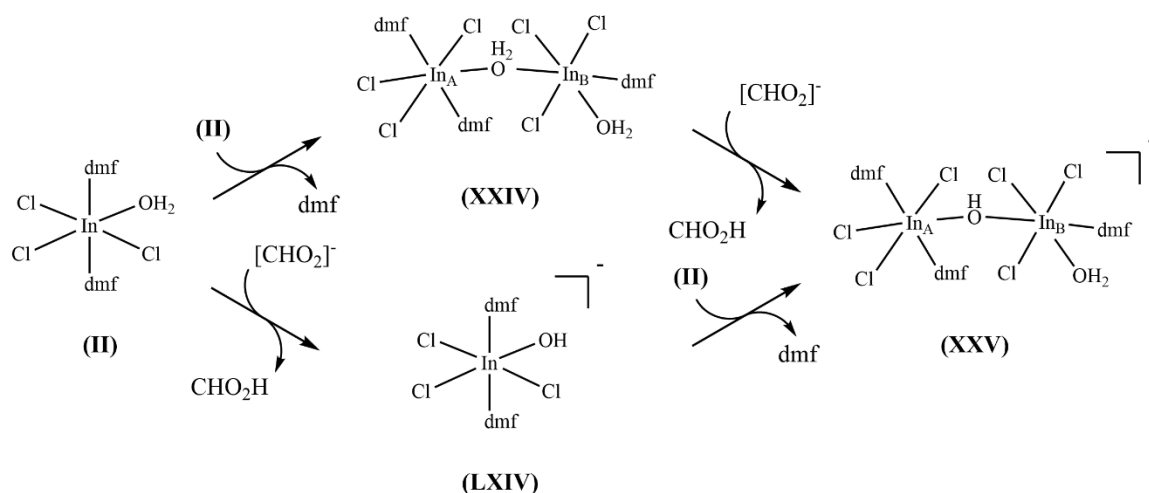
Figure 16. Scheme of original proposal and new proposal of prior water deprotonation for motif 1 of the solvated $InCl_3(H_2O)$ system. Gray represents the previously proposed mechanism, while black represents deprotonation of μ^1 water.

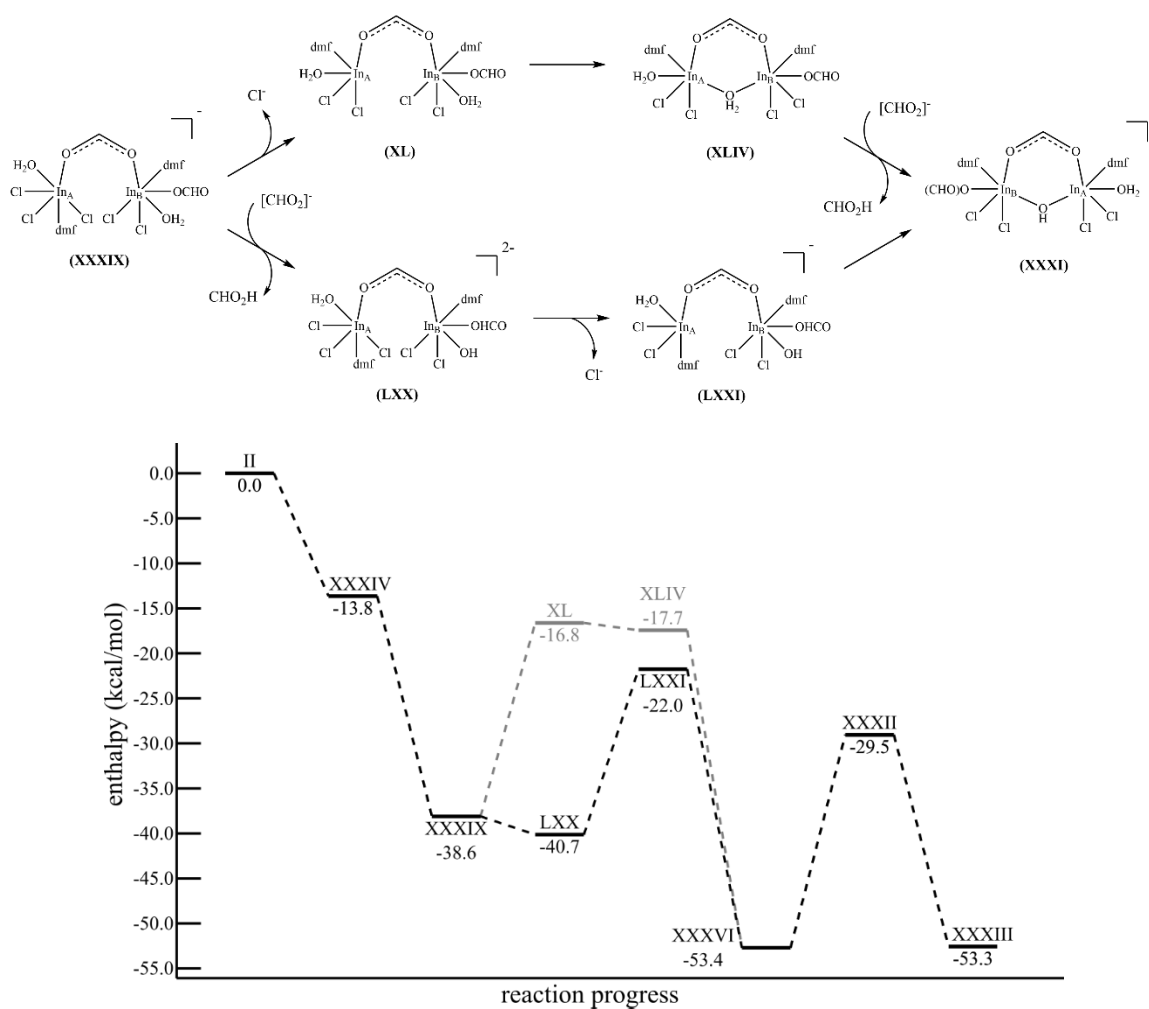For the solvated $In(NO_3)_3(H_2O)$ system, the deprotonation of the μ^1 water on **III** lowered the total enthalpy to -21.2 kcal/mol (**LXV**). Bridging **LXV** to a second equivalent of **III** using the μ^1 hydroxyl creates the already proposed **XLVI**. Seeing as deprotonation for both starting materials produced a more thermodynamically favored intermediate rather than bridging via water, this process was further assessed.
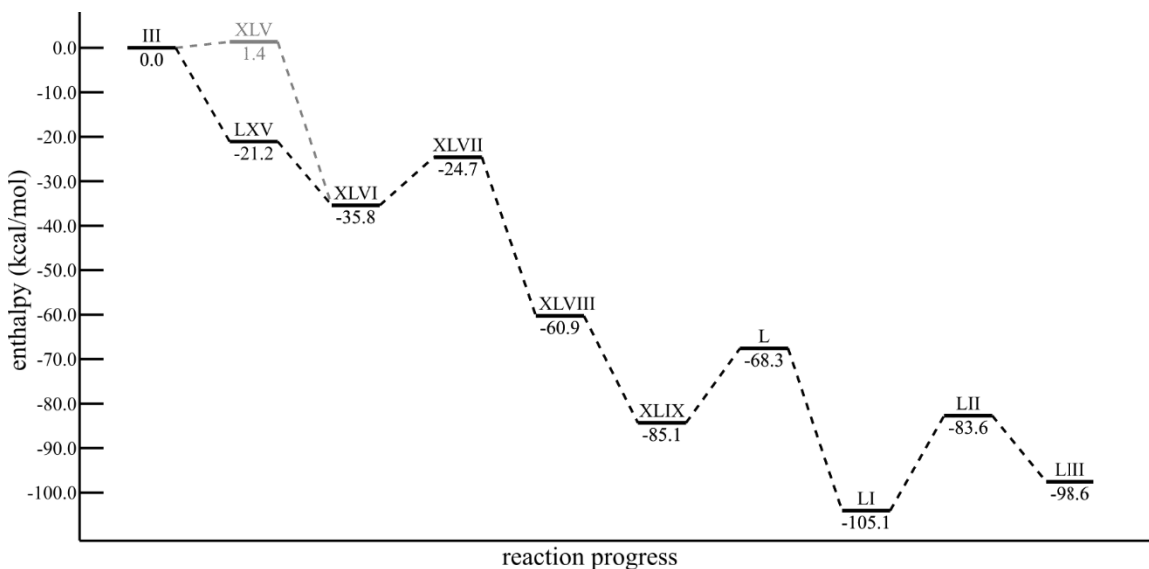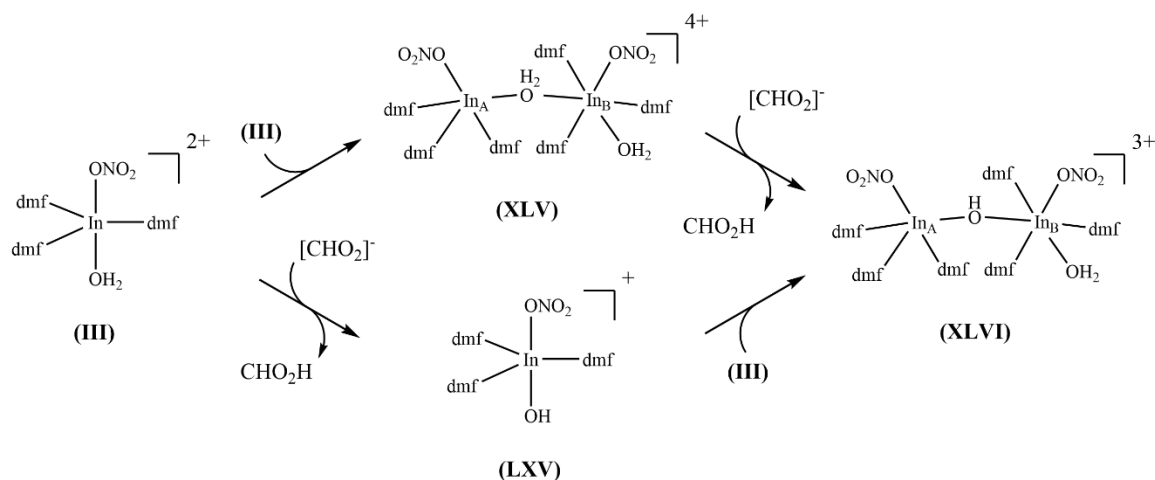
Figure 17. Scheme of original proposal and new proposal of prior water deprotonation for motif 1 of the solvated $In(NO_3)_3(H_2O)$ system. Gray represents the previously proposed mechanism, while black represents deprotonation of μ1 water.

Given the results from pathway 1 of both systems, I hypothesized that the deprotonation of u^1 water before bridging both In-atoms would be enthalpically beneficial in all of the proposed pathways. To test this, I began by deprotonating the μ^1 water of **XXXV** in pathway 2 of the solvated $InCl_3(H_2O)$ system, which was found to be 23.0 kcal/mol lower in energy than that of the previously proposed **XXXVI** (**LXVI**; H= -23.6 kcal/mol). The loss of chloride from **LXVI** then forms **LXVII** (H= -5.3 kcal/mol), which is 3.8 kcal/mol lower in enthalpy than the previously proposed **XXXVII**. The final bridging of In-atoms via a hydroxyl group creates the already proposed intermediate **XXIX**.
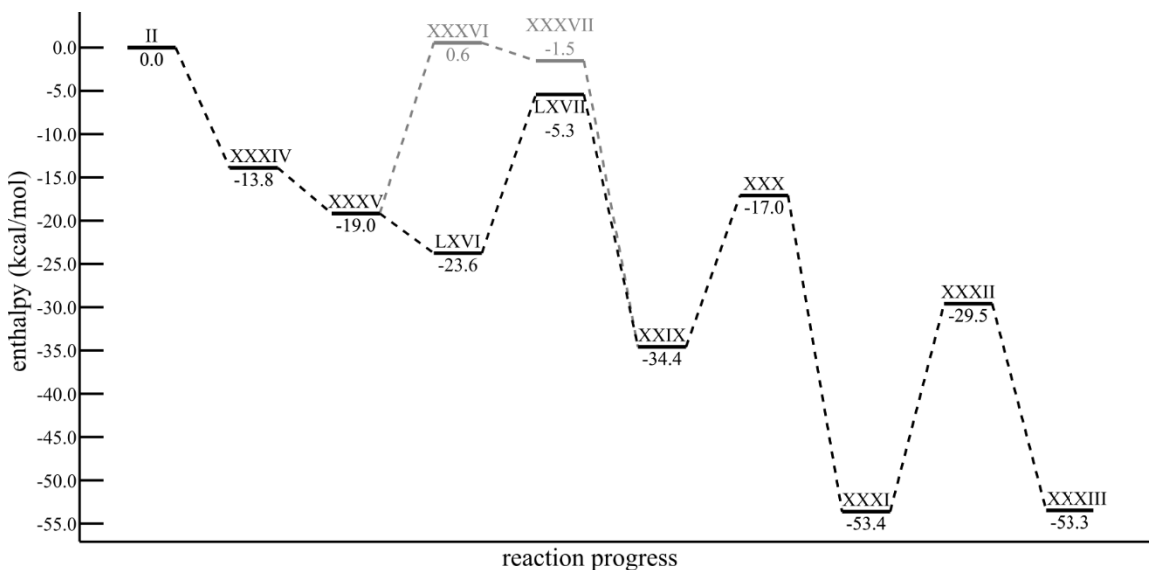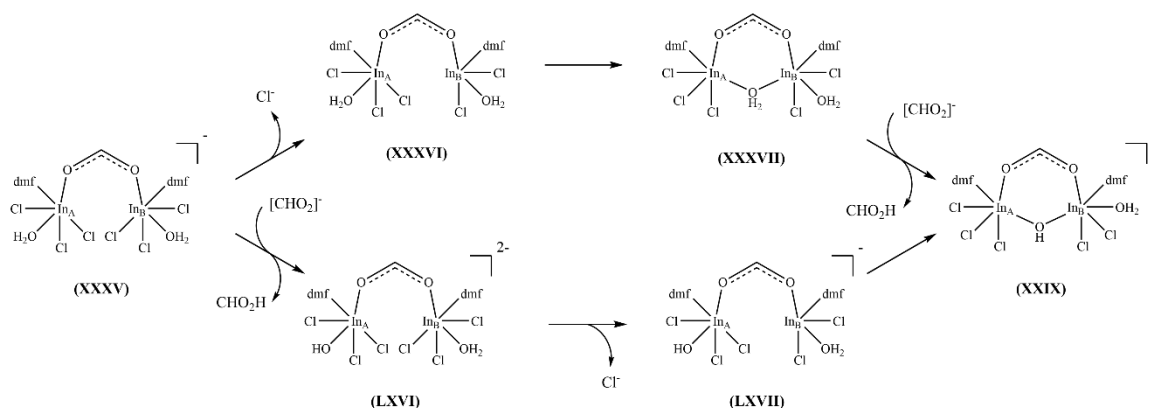
Figure 18. Scheme of original proposal and new proposal of prior water deprotonation for motif 2 of the solvated $InCl_3(H_2O)$ system. Gray represents the previously proposed mechanism, while black represents deprotonation of μ^1 water.

Similarly, pathway 3a of the solvated $InCl_3(H_2O)$ system could undergo deprotonation of the μ^1 water at intermediate **XLI** instead of the loss of a ligand. This would form intermediate **LXVIII** (H= -39.1 kcal/mol) which is 27.9 kcal/mol lower in enthalpy than the previously proposed **XLII** (H= -11.2 kcal/mol). After a loss of chloride, intermediate **LXIX** (H= -24.8 kcal/mol) would be formed which is 8.5 kcal/mol lower in enthalpy than the previously proposed **XLIII** (H= -16.3 kcal/mol). When the In-atoms become bridged by the hydroxyl group, the pathway converges on the already proposed intermediate, and final dimer, **XXXIII**.
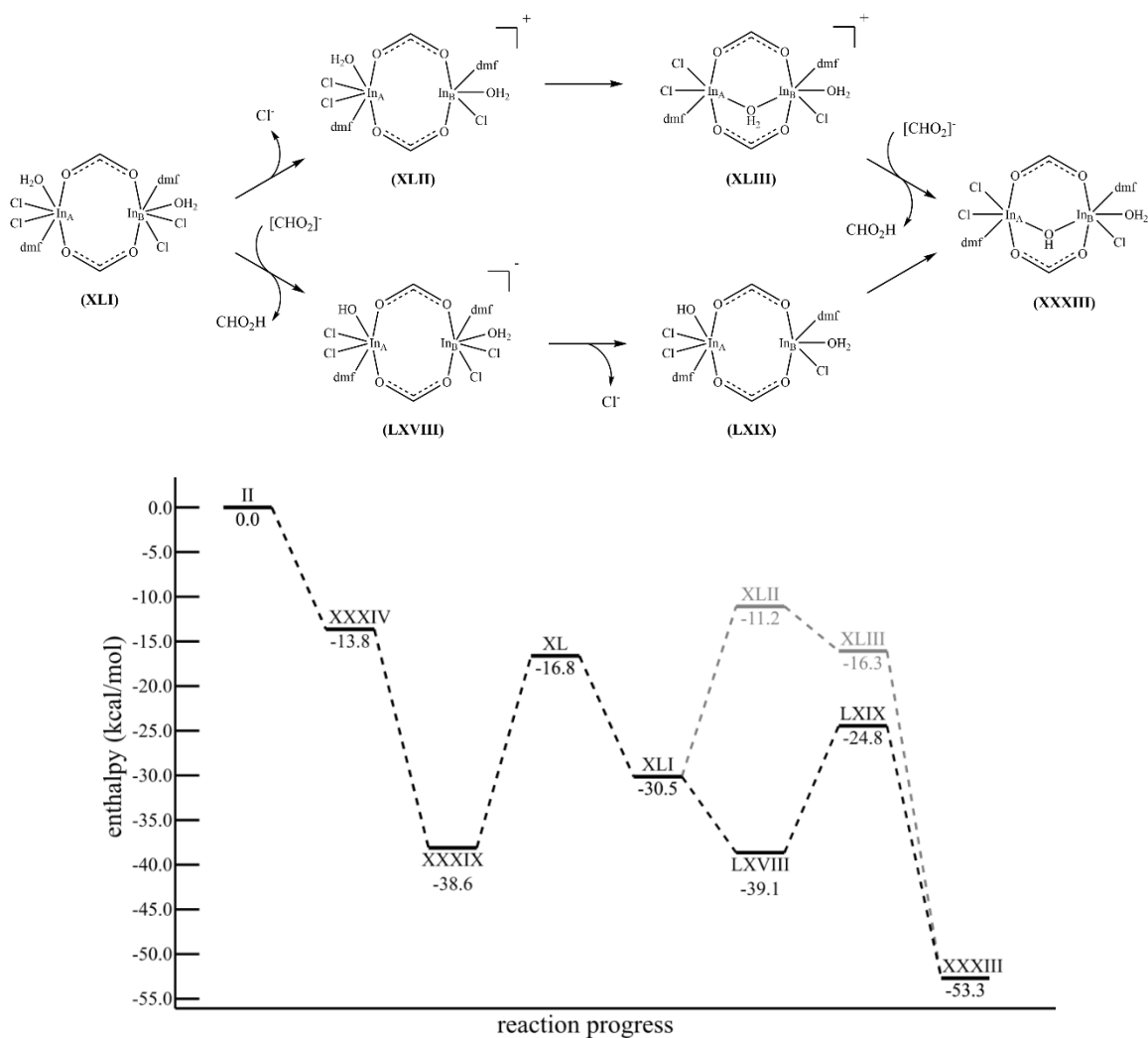
Figure 19. Scheme of original proposal and new proposal of prior water deprotonation for motif 3a of the solvated $InCl_3(H_2O)$ system. Gray represents the previously proposed mechanism, while black represents deprotonation of μ^1 water.

As for pathway 3b of the solvated $InCl_3(H_2O)$ system, the deprotonation of **XXXIX** would create **LXX** (H= -40.7 kcal/mol), which has an enthalpy that is 23.9 kcal/mol lower than the already proposed intermediate **XL** (H= -16.8 kcal/mol). Consequentially, the following loss of a chloride ligand from **LXX** would produce intermediate **LXXI** (H= -22.0 kcal/mol). This new intermediate is 4.3 kcal/mol lower than the already proposed

intermediate **XLIV** (H= -17.7 kcal/mol). Bridging both In-atoms via the hydroxide of

LXXI would produce the already proposed intermediate **XXXI**.

Figure 20. Scheme of original proposal and new proposal of prior water deprotonation for motif 3b of the solvated $InCl_3(H_2O)$ system. Gray represents the previously proposed mechanism, while black represents deprotonation of μ^1 water.

For the solvated $In(NO_3)_3(H_2O)$ system, and in addition to pathway 1, deprotonation of the μ^1 water before bridging the In-atoms in pathways 2, 3a, and 3b were also pursued. For pathway 2, if the μ^1 water of **LVII** were deprotonated, the enthalpy of formation of the product (**LXXII**) would be -34.5 kcal/mol. This value is 17.3 kcal/mol

lower than if water were to bridge first. Bridging of both In-atoms using the hydroxide of

LXXII would then produce **L** (already proposed in pathway 1 and 2).
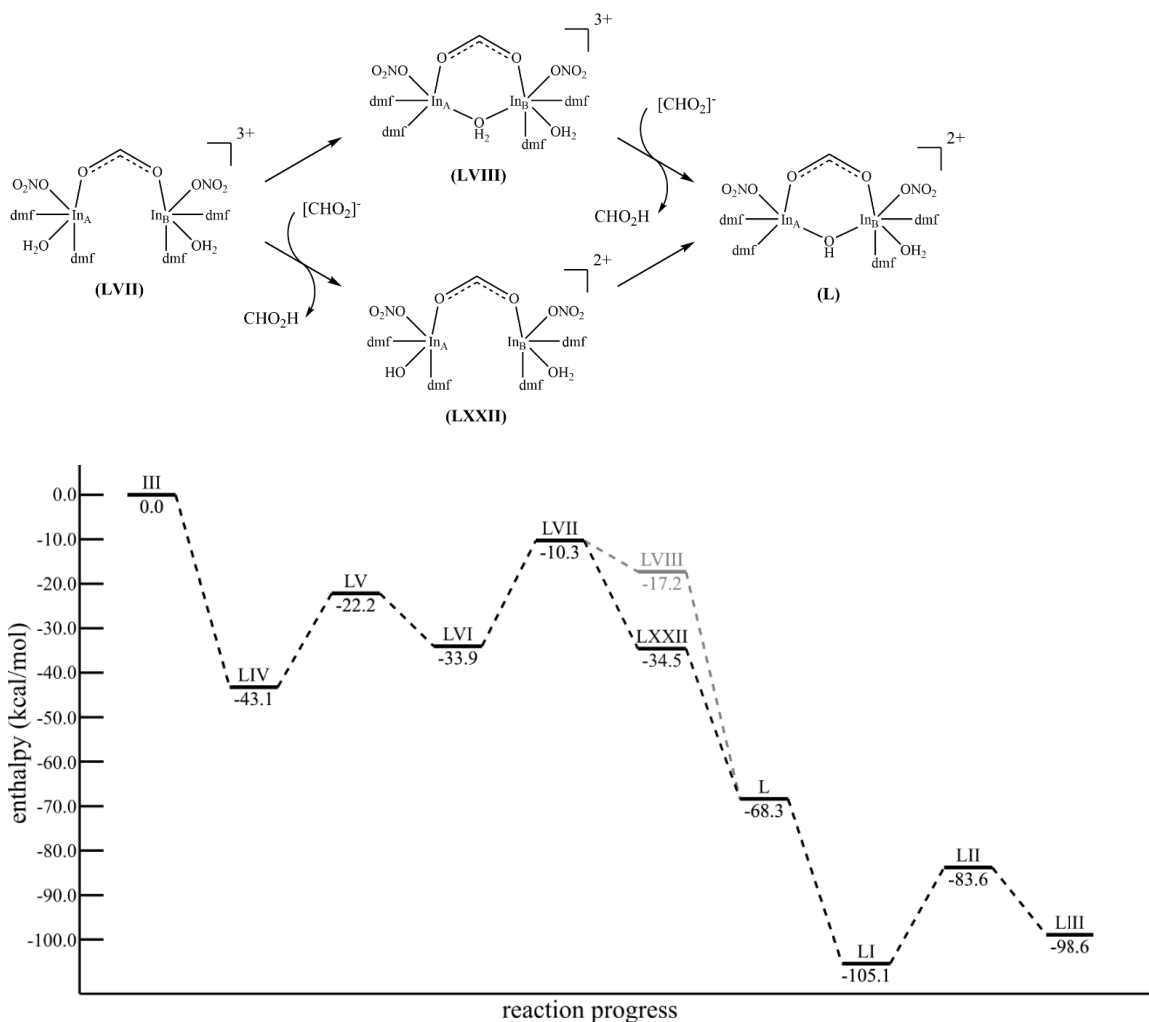
Figure 21. Scheme of original proposal and new proposal of prior water deprotonation for motif 2 of the solvated $In(NO_3)_3(H_2O)$ system. Gray represents the previously proposed mechanism, while black represents deprotonation of μ^1 water.

Pathway 3a for the solvated $In(NO_3)_3(H_2O)$ system can undergo deprotonation of

the μ^1 water before bridging the In-atoms. The product of deprotonating **LXI** would be

intermediate **LXXIII** (H= -54.7 kcal/mol). Surprisingly, this intermediate did not follow

into my hypothesis that the deprotonation of μ^1 water before bridging (regardless of the

55

system or pathway) would create intermediate(s) comparatively lower in energy. **LXXIII** is 9.8 kcal/mol higher in enthalpy than the previously proposed intermediate **LXII** (H= -64.5 kcal/mol). Bridging of both In-atoms using the hydroxide of **LXXIII** would produce the final dimer, **LIII**.
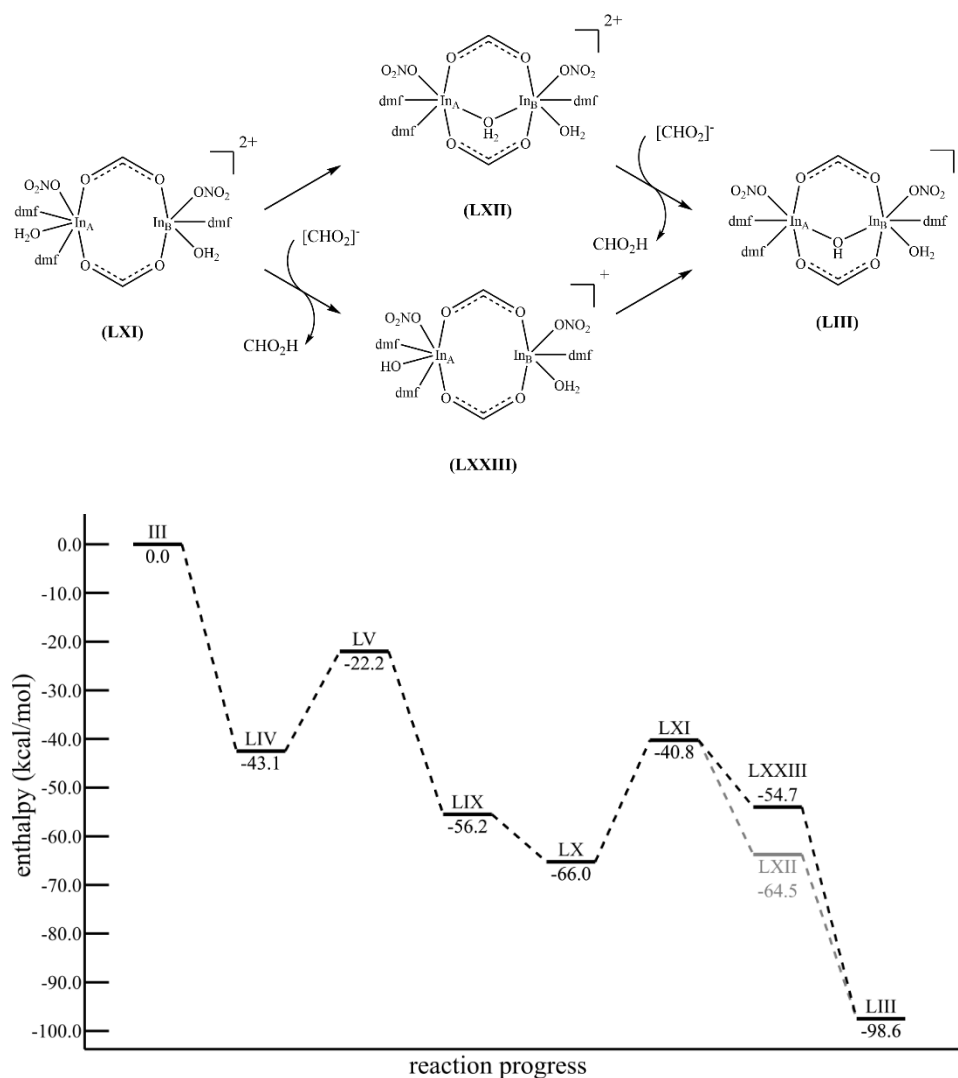
Figure 22. Scheme of original proposal and new proposal of prior water deprotonation for motif 3a of the solvated $In(NO_3)_3(H_2O)$ system. Gray represents the previously proposed mechanism, while black represents deprotonation of μ^1 water.

Pathway 3b for the solvated $In(NO_3)_3(H_2O)$ system may also undergo deprotonation of the μ^1 water before bridging the In-atoms. At intermediate **LIX** (H= -56.2

kcal/mol), the deprotonation of the μ^1 water would produce intermediate **LXXIV** (-62.2 kcal/mol); this intermediate follows the alternative deprotonation pattern of pathway 3a, and shows that deprotonating the water before bridging is 4.0 kcal/mol higher in enthalpy than the previously proposed intermediate **LXIII** (H= -66.2 kcal/mol). Bridging both In-atoms using the hydroxide of **LXXIV** would produce **LI**, which has already been proposed.
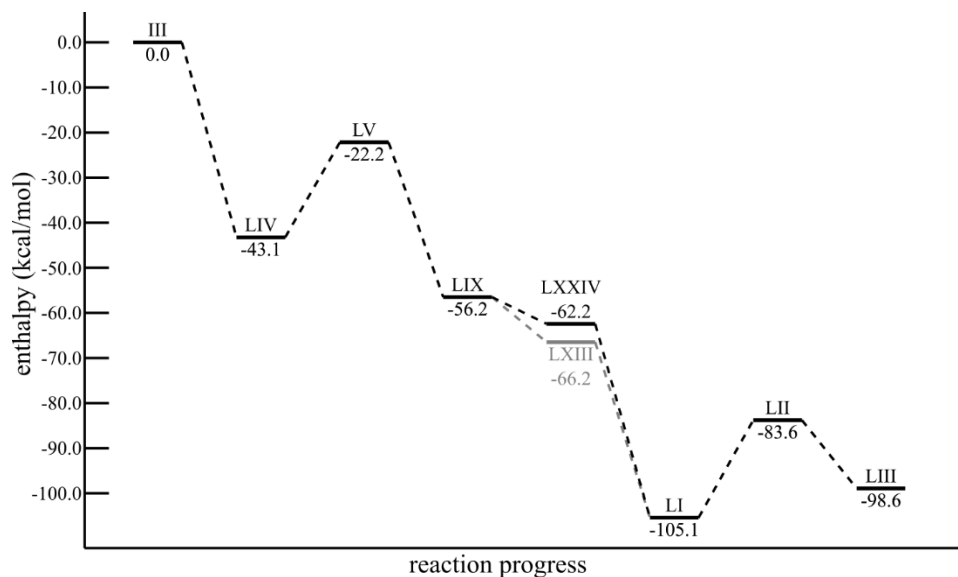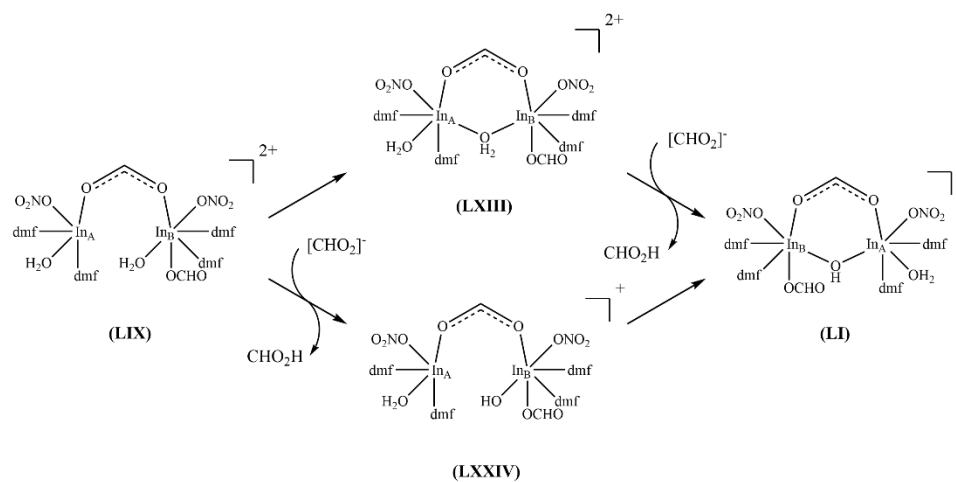
Figure 23. Scheme of original proposal and new proposal of prior water deprotonation for motif 3b of the solvated $In(NO_3)_3(H_2O)$ system. Gray represents the previously proposed mechanism, while black represents deprotonation of μ^1 water.

It is also important to note that dimerization via water and the proceeding deprotonation of the μ^2 water bridge (as originally proposed) for either system is still not enthalpically unreasonable. As explained in the methodology, when each geometry optimization calculation is completed, all raw enthalpies obtained and used are theoretically at 298.15 K, or 25 °C. In the actual synthesis of MIL-68(In) from $InCl_3(dioxane)_2(H_2O)$, for example, the reaction would be performed at temperatures upward of 120 °C [22]. This means that even if the In-atoms were bridged via water before deprotonation, achieving the "positive" enthalpy of intermediate **XXIV** (H= 10.2 kcal/mol, the intermediate with the highest enthalpy) in pathway 1 of the solvated $InCl_3(H_2O)$ system is not unlikely, and the same goes for intermediate **XLV** in pathway 1 of the solvated $In(NO_3)_3(H_2O)$ system.

Overall, there is a clear distinction between the solvated $InCl_3(H_2O)$ and solvated $In(NO_3)_3(H_2O)$ system when it comes to the ΔH's of forming the In-O-In bond. Regardless of whether deprotonation occurs before or after the In-O-In bond is made, the solvated $InCl_3(H_2O)$ system will experience an endothermic change in enthalpy followed by an exothermic change in enthalpy, or vice versa. The challenge for any proposed mechanism in the solvated $InCl_3(H_2O)$ system is how the intermediates may "escape" the low energy enthalpic well that precedes the endothermic loss of a ligand. In contrast, the solvated $In(NO_3)_3(H_2O)$ system does not need to go through the same necessary ligand loss to open a coordination site for water to bridge. As a result of nitrate acting as both a κ^1 and κ^2 ligand, there is never complete ligand dissociation, and so the system does not experience this challenge. Rather, there is a succession of exothermic changes in the relative enthalpy. This is an enthalpically favorable trait of nitrate, because as long as there is coordinated

nitrate, all proposed intermediates have an equal opportunity of remaining octahedral upon ligand dissociation; therefore, the solvated $In(NO_3)_3(H_2O)$ system appears more flexible than the solvated $InCl_3(H_2O)$ system.
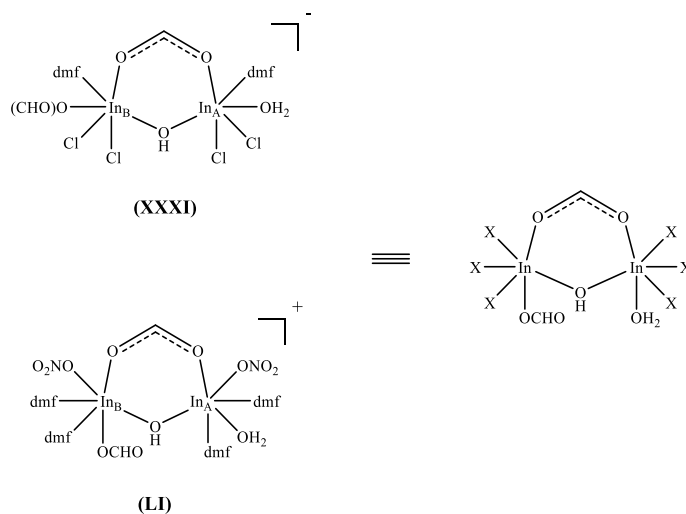
For the solvated $InCl_3(H_2O)$ system, the enthalpies of the first stable-bridged (i.e., how each bridge appears between In-atoms in the final infinite chain) intermediates were compared to see whether the hydroxyl or formate bridge is preferred to be formed first. In pathway 1, the first stable-bridged intermediate is **XXV** with an enthalpy of -21.8 kcal/mol. This bridge is an In-(μ-OH)-In bond. For pathway 2, the first stable-bridged intermediate is **XXXV** with an enthalpy of -19.0 kcal/mol. This bridge is an In-(μ-CHO$_2$)-In bond. Pathways 3a and 3b both share a common first stable-bridged species which is **XXXIX**. This intermediate contains an In-(μ-CHO$_2$)-In-(μ-CHO$_2$) bond. At first glance, the enthalpy of this intermediate (H= -38.6 kcal/mol) would exemplify twice the enthalpic favoritism over that of the first stable-bridged intermediate of pathway 1 and 2; however, the energy value should be divided by two for the two equivalents of In-monocarboxylate that were used as reactants. Doing so averages the enthalpy of **XXXIX** to -19.6 kcal/mol per In-monocarboxylate equivalent, which makes the molecule's enthalpy nearly equal to **XXV** and **XXXV**. In order of most enthalpically favored to least enthalpically favored pathway 1 would be first, pathway 3a and 3b would be second, and pathway 2 would be third. Another important aspect to take note of is that the difference between most enthalpically favored and least enthalpically favored is 1.3 kcal/mol (if using -19.6 kcal·mol^{-1}/equivalent as the "enthalpy" for intermediate **XXXIX**). So, while technically being able to rank the energy values, there is no marginally large enthalpic payoff to

forming one molecular bridge first over another, regardless of which two species come together.

The same analysis can also be applied to the solvated $In(NO_3)_3(H_2O)$ system. In pathway 1, the first stable-bridged intermediate is **XLVI**, whose enthalpy is -35.8 kcal/mol and bridge contains an In-(μ-OH)-In bond. Pathway 2's first stable-bridged intermediate is **LVI** with an enthalpy of -33.9 kcal/mol and whose molecular bridge contains an In-(μ-CHO_2$)-In bond. Also following the same motif as seen in the solvated $InCl_3(H_2O)$ system, pathway 3a and 3b for the solvated $In(NO_3)_3(H_2O)$ system share the same first stable-bridged molecule. This is intermediate **LIX** and has an enthalpy of -56.2 kcal/mol. As done previously, the value was divided by two for the two equivalents of In-monocarboxylate created at the beginning of the reaction. This yields -28.1 kcal/mol per In-monocarboxylate equivalent. If the enthalpies of these intermediates were to be ranked, pathway 1 would form the most enthalpically favored first bridge followed by pathway 2, and then pathway 3a and 3b. In this instance, the difference between the lowest and highest enthalpy is 7.7 kcal/mol (again, that is if -28.1 kcal/mol is the enthalpy used as the highest). The difference in enthalpies between the highest and lowest first stable-bridged intermediates appears to more significant for the solvated $In(NO_3)_3(H_2O)$ system than for the solvated $InCl_3(H_2O)$ system; however, this is a result of constraining certain atomic cartesian coordinates of various intermediates described in the methodology. The difference is then made out to be not as drastic, and becomes interesting even more so as constraining the coordinates has only increased the difference slightly in comparison to that of the solvated $InCl_3(H_2O)$ system.

The lowest-enthalpy intermediate among all pathways in the solvated $InCl_3(H_2O)$ system is **XXXI**. Structure **XXXI** is the point at which three out of four pathway motifs converge (those being pathway 1, 2, and 3b). As for the solvated $In(NO_3)_3(H_2O)$ system, the lowest-enthalpy intermediate among all pathways is **LI** and is also a convergence point for the same three pathway motifs. When these two intermediates are compared, they are structurally similar if the coordinatively saturating ligands and charge balancing ligands were to be excluded. For both **XXXI** and **LI**, there are two bridges that connect both In-atoms which consist of a μ^2 carboxylate and a μ^2 hydroxyl group. So, while motif 3a is enthalpically valid, it can possibly be excluded as a mechanism of action for both the solvated $InCl_3(H_2O)$ and solvated $In(NO_3)_3(H_2O)$ system as there is no similar intermediate to that of **XXXI** and **LI**.

Figure 24. The comparison of **576** from the solvated $InCl_3(H_2O)$ system and **541** from the solvated $In(NO_3)_3(H_2O)$ system. X is used as a generic placeholder ligand, so the structural similarities are clearer.
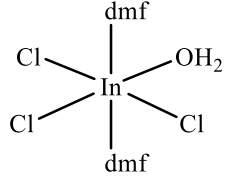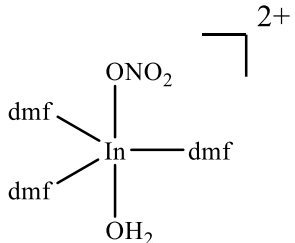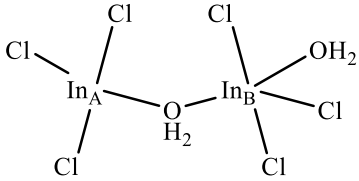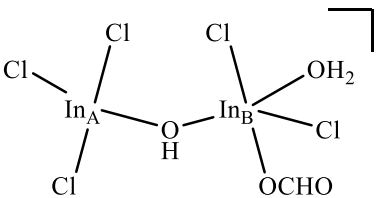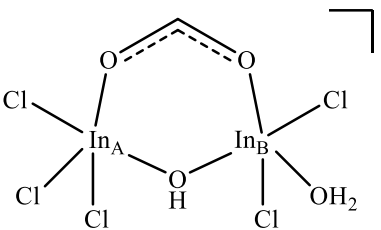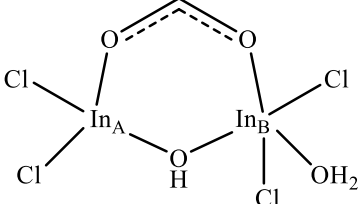
IV.   Conclusions
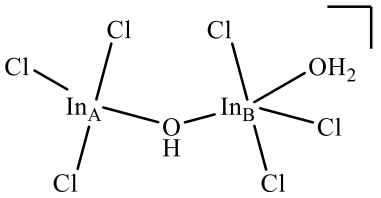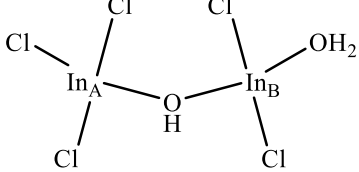
After determining the relative enthalpies of formation for the various intermediates in motifs 1, 2, 3a, and 3b of the unsolvated $InCl_3(H_2O)$, solvated $InCl_3(H_2O)$, and solvated $In(NO_3)_3(H_2O)$ systems, this work supports previous claims that In-dimerization may occur via an In-monocarboxylate PNBU before additional self-assembly of the In-infinite chain. Additionally, it was found that forming a hydroxyl bridge, regardless of the system, has nearly the same relative enthalpy as does the formation of an In-(μ-CHO_2)-In bridge. Being that the first stable-bridged intermediates in the solvated $InCl_3(H_2O)$ are equal in enthalpy, it is indicative of the system's desire to simply bring together two In-atoms without majorly prioritizing what molecule bridges them. The same can be said for the solvated $In(NO_3)_3(H_2O)$ system.

Additionally, studies on the deprotonation of water (which forms the hydroxyl bridge between In-atoms) exemplifies another similar trend for both solvated systems. If water is deprotonated before creating the In-O-In bond, the relative enthalpies of the following 1 or 2 intermediates (for the solvated $In(NO_3)_3(H_2O)$ and solvated $InCl_3(H_2O)$ systems, respectively) are reduced. Two of these such intermediates are **XXXI** and **LI**, and are found to be the intermediates with the lowest relative enthalpies among all proposed intermediates in the solvated systems. Both of these intermediates are a convergence point within motif 1, 2, and 3b. This shows that indium can possess multiple methods of initial dimerization from different starting materials, and still converge on one favorable structure (in this case being an In-dimer bridged by one formate and one hydroxyl bridge). While I originally hypothesized that a single formate or hydroxyl mechanism would be responsible for the formation of the In-infinite chain SBU, similar enthalpic intermediate values allow
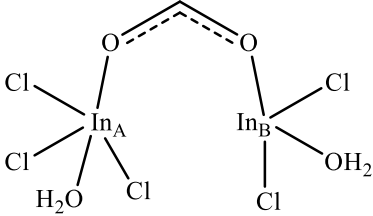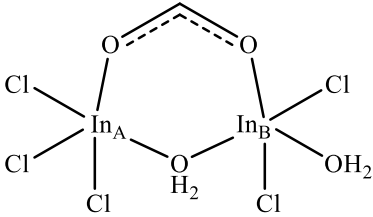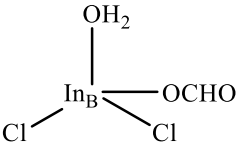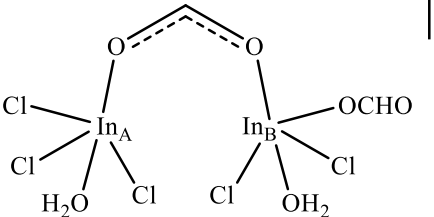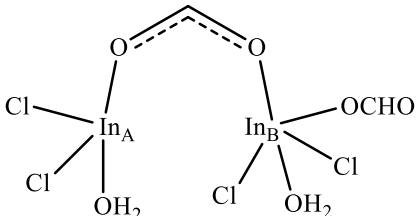
me to hypothesize that motif 1, 2, 3a, and 3b work alongside one another with a weighted

distribution as to support MOF self-assembly growth and reparation.

Appendix I

Molecule No.	Molecular Structure	Enthalpy (kcal/mol)	Lot No.
I	InCl$_3$(H$_2$O)	-915492.266	VTD-E-1
II		-1227183.821	VTD-E-526
III		-692312.197	VTD-F-440
IV		-1830991.853	VTD-E-515
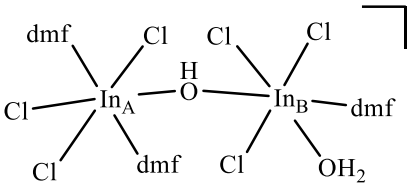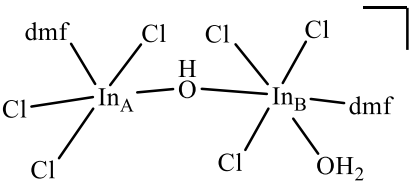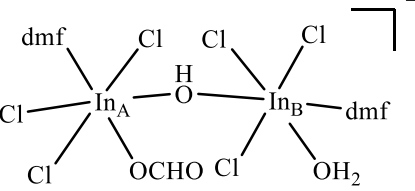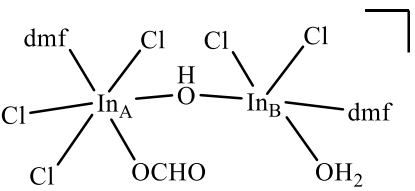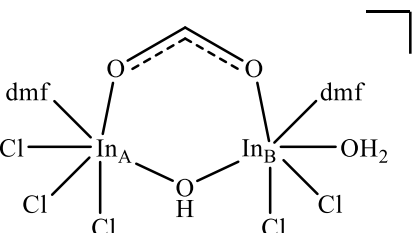
V		-1830747.743	VTD-E-516
VI		-1541857.331	VTD-E-517
VII		-1660629.245	VTD-E-136
VIII		-1660638.266	VTD-E-147
IX		-1371751.881	VTD-E-152
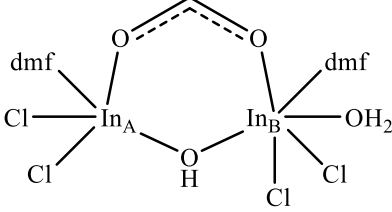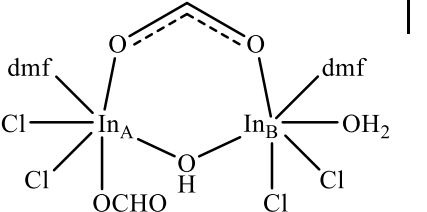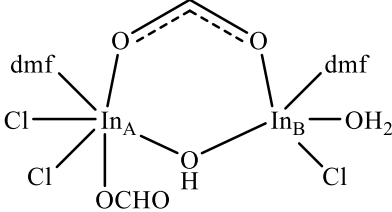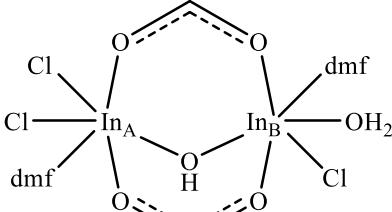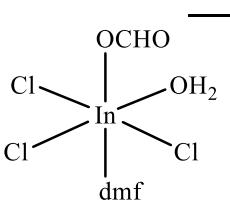
X		-1490518.851	VTD-E-155
XI		-1490528.548	VTD-E-368
XII		-1201641.182	VTD-E-174
XIII		-1034250.465	VTD-E-188
XIV		-1949771.125	VTD-E-431

XV		-1660879.351	VTD-E-432
XVI		-1660889.564	VTD-E-250
XVII		-745365.739	VTD-E-356
XVIII		-1779644.079	VTD-E-352
XIX		-1490752.461	VTD-E-354

XX		-1490768.636	VTD-E-430

Structure XX: Cl, H₂O—In_A—Cl, O, O, In_B—OH₂, Cl (bridged formate/CHO groups)

Cl—In_A with H₂O and Cl; In_B with OH₂ and Cl; bridged by two O=CH—O units.

| XXI | | -1490782.157 | VTD-E-369 |

Structure XXI: Cl, Cl—In_A; In_B—OH₂, Cl; bridging O's and O H₂.

| XXII | | -1490747.357 | VTD-E-617 |

Structure XXII: Cl, Cl—In_A—OH₂; In_B—Cl, Cl, OCHO; bridging O H₂.

| XXIII | | -1071339.859 | VTD-E-525 |

Structure XXIII: dmf, Cl—In—Cl, Cl, OH₂.

| XXIV | | -2298533.758 | VTD-E-585 |

Structure XXIV: dmf, Cl—In_A—Cl, Cl, dmf; O H₂ bridge; Cl, Cl—In_B—dmf, OH₂.
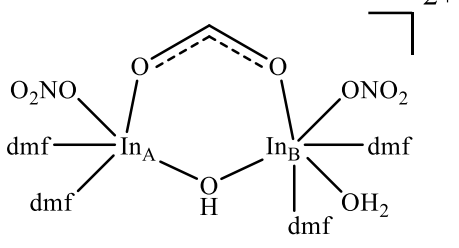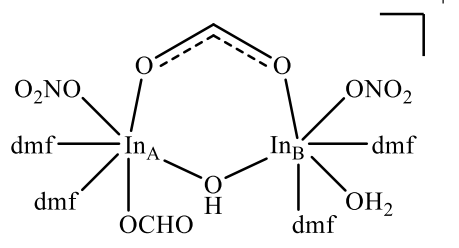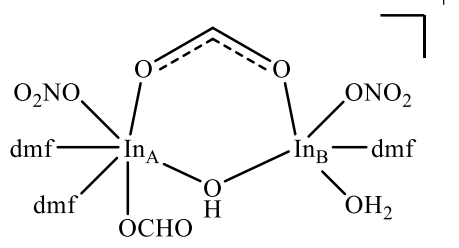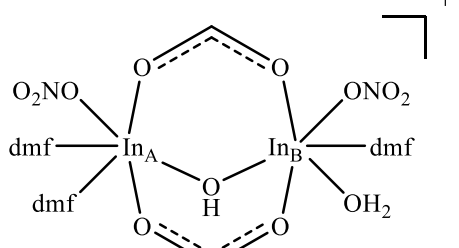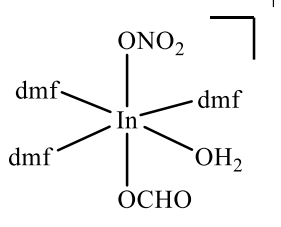
XXV	dmf, Cl, Cl, Cl / Cl—In$_A$—O(H)—In$_B$—dmf / Cl, dmf, Cl, OH$_2$ ⁻	-2298273.768	VTD-E-586
XXVI	dmf, Cl, Cl, Cl / Cl—In$_A$—O(H)—In$_B$—dmf / Cl, Cl, OH$_2$ ⁻	-2142431.809	VTD-E-587
XXVII	dmf, Cl, Cl, Cl / Cl—In$_A$—O(H)—In$_B$—dmf / Cl, OCHO, Cl, OH$_2$ 2-	-2261185.720	VTD-E-588
XXVIII	dmf, Cl, Cl, Cl / Cl—In$_A$—O(H)—In$_B$—dmf / Cl, OCHO, OH$_2$ ⁻	-1972308.728	VTD-E-589
XXIX	O=·····=O bridging / dmf, Cl, Cl, Cl—In$_A$—O(H)—In$_B$—OH$_2$, dmf, Cl ⁻	-1972321.836	VTD-E-573
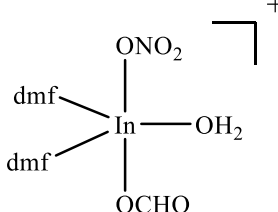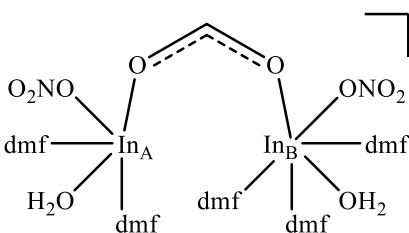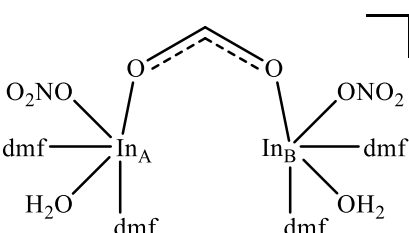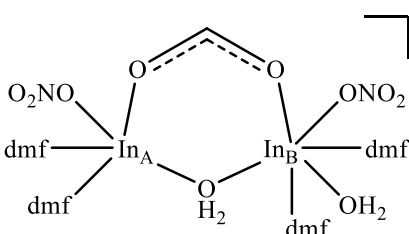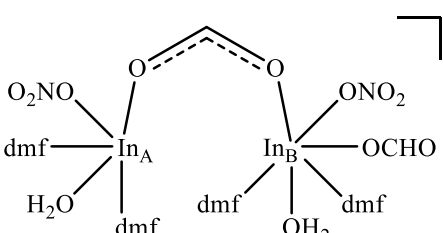
XXX		-1683443.779	VTD-E-574
XXXI		-1802199.351	VTD-E-576
XXXII		-1513314.818	VTD-E-578
XXXIII		-1513338.615	VTD-E-538
XXXIV		-1190093.068	VTD-E-544

XXXV		-2261458.474	VTD-E-570
XXXVI		-1972578.158	VTD-E-571
XXXVII		-1972580.300	VTD-E-572
XXXVIII		-901213.877	VTD-E-543
XXXIX		-2091336.530	VTD-E-580
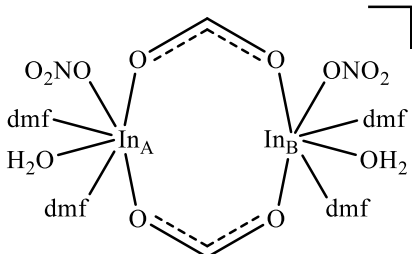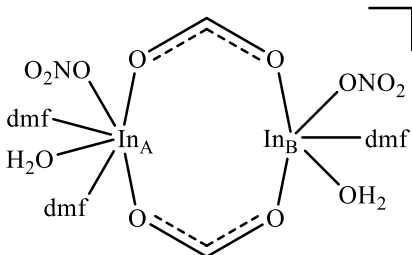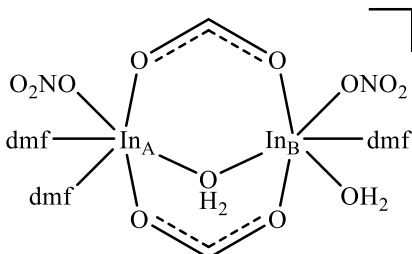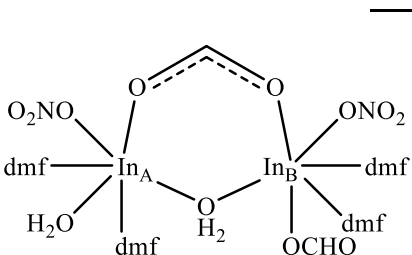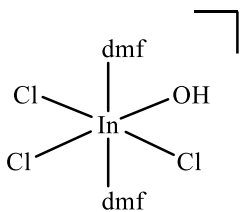
XL	H₂O, Cl, Cl, dmf, In$_A$; O=...=O; dmf, OCHO, OH₂, Cl, Cl, In$_B$	-1802454.083	VTD-E-581
XLI	H₂O, Cl, Cl, dmf, In$_A$; O=...=O, O=...=O; dmf, OH₂, Cl, Cl, In$_B$	-1802467.819	VTD-E-582
XLII	H₂O, Cl, Cl, dmf, In$_A$; O=...=O, O=...=O; dmf, OH₂, Cl, In$_B$ [+]	-1513587.844	VTD-E-583
XLIII	Cl, Cl, dmf, In$_A$; O=...=O, O(H₂), O=...=O; dmf, OH₂, Cl, In$_B$ [+]	-1513592.907	VTD-E-584
XLIV	dmf, H₂O, Cl, Cl, In$_A$; O=...=O, O(H₂); dmf, OCHO, Cl, Cl, In$_B$	-1802455.022	VTD-E-601

72
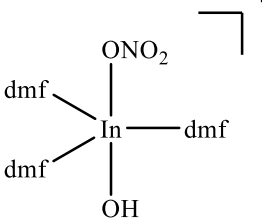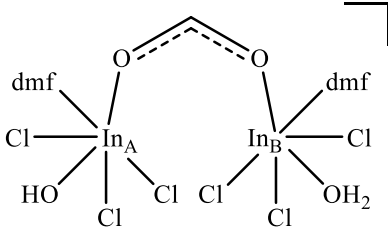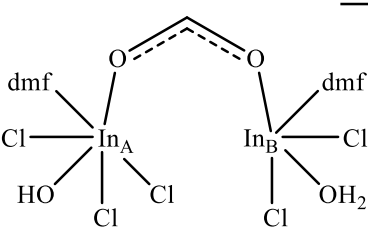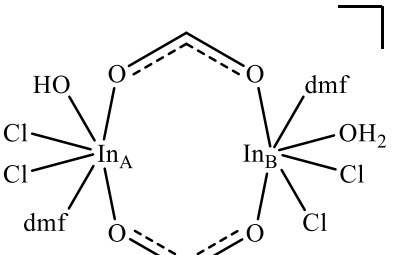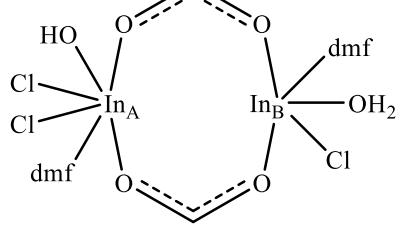
XLV	O$_2$NO, dmf, dmf, In$_A$—O(H$_2$)—In$_B$, dmf, ONO$_2$, dmf, OH$_2$	4+	-1384622.952	VTD-F-574
XLVI	O$_2$NO, dmf, dmf, In$_A$—O(H)—In$_B$, dmf, ONO$_2$, dmf, OH$_2$	3+	-1384368.809	VTD-F-617
XLVII	O$_2$NO, dmf, dmf, In$_A$—O(H)—In$_B$, dmf, ONO$_2$, OH$_2$	3+	-1228534.056	VTD-F-576
XLVIII	O$_2$NO, (CHO)O, dmf, dmf, In$_A$—O(H)—In$_B$, dmf, ONO$_2$, OH$_2$	2+	-1347289.454	VTD-F-558
XLIX	O$_2$NO, dmf, dmf, In$_A$—O(H)—In$_B$, dmf, dmf, ONO$_2$, OH$_2$	2+	-1347313.594	VTD-F-548
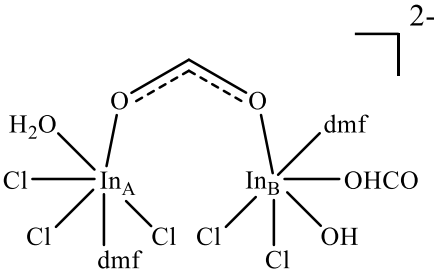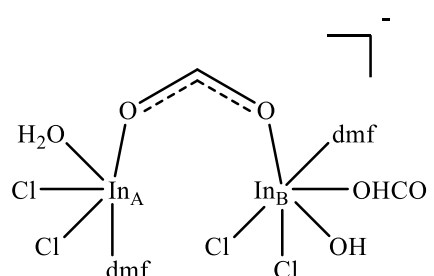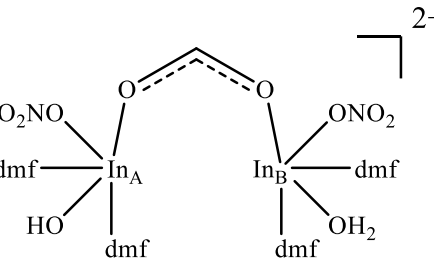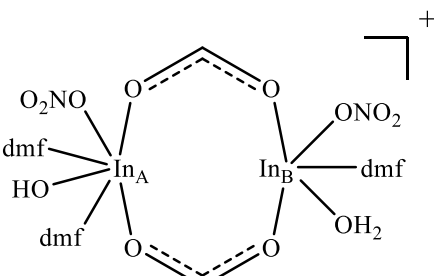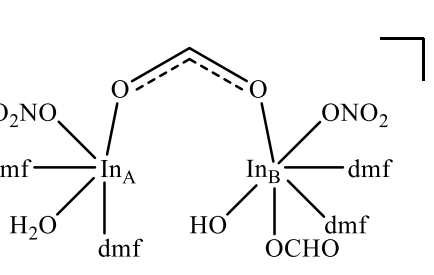
L	$2+$	-1191473.180	VTD-F-561
LI	$+$	-1310229.152	VTD-F-541
LII	$+$	-1154383.926	VTD-F-614
LIII	$+$	-1154398.931	VTD-F-613
LIV	$+$	-811074.466	VTD-F-537
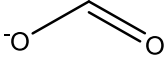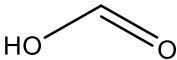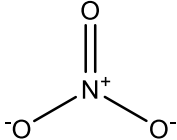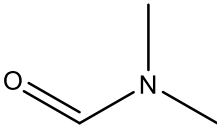
LV	ONO₂ / dmf—In—OH₂ / dmf / OCHO (charge +)	-655229.878	VTD-F-535
LVI	(charge 3+) O_2NO, dmf—In_A—, H_2O, dmf bridged to In_B—dmf, OH_2, dmf via O=...=O, ONO_2	-1347553.740	VTD-F-538
LVII	(charge 3+) O_2NO, dmf—In_A—, H_2O, dmf bridged to In_B—dmf, OH_2, dmf via O=...=O, ONO_2	-1191706.506	VTD-F-536
LVIII	(charge 3+) O_2NO, dmf—In_A—, dmf, In_A—OH_2—In_B bridge, dmf, OH_2, ONO_2	-1191713.399	VTD-F-560
LIX	(charge 2+) O_2NO, dmf—In_A—, H_2O, dmf bridged to In_B—OCHO, dmf, OH_2 via O=...=O, ONO_2	-1310471.613	VTD-F-549

LX	[structure: dinuclear In complex]$^{2+}$	-1310481.353	VTD-F-550
LXI	[structure: dinuclear In complex]$^{2+}$	-1154632.515	VTD-F-615
LXII	[structure: dinuclear In complex]$^{2+}$	-1154656.236	VTD-F-616
LXIII	[structure: dinuclear In complex]$^{2+}$	-1310481.528	VTD-F-563
LXIV	[structure: In complex]$^{-}$	-1226896.623	VTD-E-607

LXV	ONO₂ structure with In center, dmf, dmf, dmf, OH (charge +)	-692042.095	VTD-F-577
LXVI	In_A / In_B bridged structure (charge 2-)	-2261171.692	VTD-E-630
LXVII	In_A / In_B bridged structure (charge -)	-1972292.785	VTD-E-631
LXVIII	In_A / In_B double-bridged structure (charge -)	-1802185.058	VTD-E-634
LXIX	In_A / In_B double-bridged structure	-1513310.089	VTD-E-635

LXX		-2091047.310	VTD-E-632
LXXI		-1802167.953	VTD-E-636
LXXII		-1191439.333	VTD-F-618
LXXIII		-1154355.032	VTD-F-619
LXXIV		-1310186.224	VTD-F-622

LXXV		-118719.152	VTD-E-23
LXXVI		-119010.499	VTD-E-569
LXXVII	Cl⁻	-288875.030	VTD-E-26
LXXVIII		-175902.340	VTD-F-15
LXXIX		-155823.662	VTD-G-3

References

(1)   Li, H.; Eddaoudi, M.; O'Keeffe, M.; Yaghi, O. M. Design and Synthesis of an exceptionally Stable and Highly Metal-Organic Framework. *Nature* **1999**, *402*, 276–279.

(2)   Hong, D. H.; Shim, H. S.; Ha, J.; Moon, H. R. MOF-on-MOF Architectures: Applications in Separation, Catalysis, and Sensing. *Bulletin of the Korean Chemical Society*. John Wiley and Sons Inc July 1, 2021, pp 956–969. https://doi.org/10.1002/bkcs.12335.

(3)   Li, M.; Li, D.; O'Keeffe, M.; Yaghi, O. M. Topological Analysis of Metal-Organic Frameworks with Polytopic Linkers and/or Multiple Building Units and the Minimal Transitivity Principle. *Chemical Reviews*. January 22, 2014, pp 1343–1370. https://doi.org/10.1021/cr400392k.

(4)   Gonzalez-Nelson, A.; Coudert, F. X.; van der Veen, M. A. Rotational Dynamics of Linkers in Metal–Organic Frameworks. *Nanomaterials*. MDPI AG March 1, 2019. https://doi.org/10.3390/nano9030330.

(5)   Kalmutzki, M. J.; Hanikel, N.; Yaghi, O. M. *Secondary Building Units as the Turning Point in the Development of the Reticular Chemistry of MOFs*; 2018; Vol. 4.

(6)   Zahn, D. Thermodynamics and Kinetics of Prenucleation Clusters, Classical and Non-Classical Nucleation. *Chemphyschem* **2015**, *16* (10), 2069–2075.

(7)   Embrechts, H.; Embrechts, H.; Kriesten, M.; Ermer, M.; Peukert, W.; Peukert, W.; Hartmann, M.; Hartmann, M.; Distaso, M.; Distaso, M. Role of Prenucleation Building Units in Determining Metal-Organic Framework MIL-53(Al) Morphology. *Cryst Growth Des* **2020**, *20* (6), 3641–3649. https://doi.org/10.1021/acs.cgd.9b01384.

(8)   Moosavi, S. M.; Nandy, A.; Jablonka, K. M.; Ongari, D.; Janet, J. P.; Boyd, P. G.; Lee, Y.; Smit, B.; Kulik, H. J. Understanding the Diversity of the Metal-Organic Framework Ecosystem. *Nat Commun* **2020**, *11* (1). https://doi.org/10.1038/s41467-020-17755-8.

(9)   Luo, Y.; Bag, S.; Zaremba, O.; Cierpka, A.; Andreo, J.; Wuttke, S.; Friederich, P.; Tsotsalas, M. MOF Synthesis Prediction Enabled by Automatic Data Mining and Machine Learning**. *Angewandte Chemie International Edition* **2022**, *61* (19), e202200242. https://doi.org/https://doi.org/10.1002/anie.202200242.

(10)   Glasby, L. T.; Gubsch, K.; Bence, R.; Oktavian, R.; Isoko, K.; Moosavi, S. M.; Cordiner, J. L.; Cole, J. C.; Moghadam, P. Z. DigiMOF: A Database of Metal–Organic Framework Synthesis Information Generated via Text Mining. *Chemistry*

of Materials **2023**, *35* (11), 4510–4524.
https://doi.org/10.1021/acs.chemmater.3c00788.

(11)   Islamoglu, T.; Goswami, S.; Li, Z.; Howarth, A. J.; Farha, O. K.; Hupp, J. T.
Postsynthetic Tuning of Metal-Organic Frameworks for Targeted Applications.
Acc Chem Res **2017**, *50* (4), 805–813.
https://doi.org/10.1021/acs.accounts.6b00577.

(12)   Ha, J.; Lee, J. H.; Moon, H. R. Alterations to Secondary Building Units of Metal-
Organic Frameworks for the Development of New Functions. *Inorganic Chemistry
Frontiers*. Royal Society of Chemistry January 7, 2019, pp 12–27.
https://doi.org/10.1039/c9qi01119f.

(13)   Kuppler, R. J.; Timmons, D. J.; Fang, Q. R.; Li, J. R.; Makal, T. A.; Young, M. D.;
Yuan, D.; Zhao, D.; Zhuang, W.; Zhou, H. C. Potential Applications of Metal-
Organic Frameworks. *Coordination Chemistry Reviews*. December 2009, pp
3042–3066. https://doi.org/10.1016/j.ccr.2009.05.019.

(14)   Raptopoulou, C. P. Metal-Organic Frameworks: Synthetic Methods and Potential
Applications. *Materials*. MDPI AG January 2, 2021, pp 1–32.
https://doi.org/10.3390/ma14020310.

(15)   Defuria, M. D.; Zeller, M.; Genna, D. T. Removal of Pharmaceuticals from Water
via π-π Stacking Interactions in Perfluorinated Metal-Organic Frameworks. *Cryst
Growth Des* **2016**, *16* (6), 3530–3534. https://doi.org/10.1021/acs.cgd.6b00488.

(16)   Geisse, A. R.; Ngule, C. M.; Genna, D. T. Removal of Lead Ions from Water
Using Thiophene-Functionalized Metal-Organic Frameworks. *Chemical
Communications* **2019**, *56* (2), 237–240. https://doi.org/10.1039/c9cc09022c.

(17)   Dechellis, D. M.; Ngule, C. M.; Genna, D. T. Removal of Hydrocarbon
Contaminants from Water with Perfluorocarboxylated UiO-6: X Derivatives. *J
Mater Chem A Mater* **2020**, *8* (12), 5848–5852.
https://doi.org/10.1039/c9ta11144a.

(18)   Downs, A. J.; Himmel, H.-J. New Light on the Chemistry of the Group 13 Metals.
In *The Group 13 Metals Aluminium, Gallium, Indium and Thallium: Chemical
Patterns and Peculiarities*; John Wiley & Sons, Ltd, 2011; pp 1–74.
https://doi.org/10.1002/9780470976548.ch1.

(19)   Aguirre-Díaz, L. M.; Reinares-Fisac, D.; Iglesias, M.; Gutiérrez-Puebla, E.;
Gándara, F.; Snejko, N.; Monge, M. Á. Group 13th Metal-Organic Frameworks
and Their Role in Heterogeneous Catalysis. *Coordination Chemistry Reviews*.
Elsevier B.V. March 15, 2017, pp 1–27. https://doi.org/10.1016/j.ccr.2016.12.003.

(20)   Gislason, M.; Lloyd, M. H.; Tuck, D. G. Coordination Compounds of Indium. X.
Anionic Indium(III) Halide Complexes. *Inorg Chem* **1971**, *10* (9), 1907–1910.

(21)   Zheng, S. T.; Bu, J. J.; Wu, T.; Chou, C.; Feng, P.; Bu, X. Porous Indium-Organic Frameworks and Systematization of Structural Building Blocks. *Angewandte Chemie - International Edition* **2011**, *50* (38), 8858–8862. https://doi.org/10.1002/anie.201101957.

(22)   Tatebe, C. J.; Yusuf, S.; Bellas, M. K.; Zeller, M.; Arntsen, C.; Genna, D. T. On the Role of Dioxane in the Synthesis of In-Derived MOFs. *Cryst Growth Des* **2021**, *21* (12), 6840–6846. https://doi.org/10.1021/acs.cgd.1c00766.

(23)   Volkringer, C.; Meddouri, M.; Loiseau, T.; Guillou, N.; Marrot, J.; Férey, G.; Haouas, M.; Taulelle, F.; Audebrand, N.; Latroche, M. The Kagomé Topology of the Gallium and Indium Metal-Organic Framework Types with a MIL-68 Structure: Synthesis, XRD, Solid-State NMR Characterizations, and Hydrogen Adsorption. *Inorg Chem* **2008**, *47* (24), 11892–11901. https://doi.org/10.1021/ic801624v.

(24)   Forgan, R. S. Modulated Self-Assembly of Metal-Organic Frameworks. *Chemical Science*. Royal Society of Chemistry May 14, 2020, pp 4546–4562. https://doi.org/10.1039/d0sc01356k.

(25)   Avci, C.; Imaz, I.; Carné-Sánchez, A.; Pariente, J. A.; Tasios, N.; Pérez-Carvajal, J.; Alonso, M. I.; Blanco, A.; Dijkstra, M.; López, C.; Maspoch, D. Self-Assembly of Polyhedral Metal–Organic Framework Particles into Three-Dimensional Ordered Superstructures. *Nat Chem* **2018**, *10* (1), 78–84. https://doi.org/10.1038/nchem.2875.

(26)   Sinnwell, M. A.; Miller, Q. R. S.; Palys, L.; Barpaga, D.; Liu, L.; Bowden, M. E.; Han, Y.; Ghose, S.; Sushko, M. L.; Schaef, H. T.; Xu, W.; Nyman, M.; Thallapally, P. K. Molecular Intermediate in the Directed Formation of a Zeolitic Metal-Organic Framework. *J Am Chem Soc* **2020**, *142* (41), 17598–17606. https://doi.org/10.1021/jacs.0c07862.

(27)   Peng, L.; Yang, S.; Jawahery, S.; Moosavi, S. M.; Huckaba, A. J.; Asgari, M.; Oveisi, E.; Nazeeruddin, M. K.; Smit, B.; Queen, W. L. Preserving Porosity of Mesoporous Metal-Organic Frameworks through the Introduction of Polymer Guests. *J Am Chem Soc* **2019**, *141* (31), 12397–12405. https://doi.org/10.1021/jacs.9b05967.

(28)   Loiseau, T.; Serre, C.; Huguenard, C.; Fink, G.; Taulelle, F.; Henry, M.; Bataille, T.; Férey, G. A Rationale for the Large Breathing of the Porous Aluminum Terephthalate (MIL-53) Upon Hydration. *Chemistry - A European Journal* **2004**, *10* (6), 1373–1382. https://doi.org/10.1002/chem.200305413.

(29)   Anokhina, E. V.; Vougo-Zanda, M.; Wang, X.; Jacobson, A. J. In(OH)BDC·0.75BDCH2 (BDC = Benzenedicarboxylate), a Hybrid Inorganic-Organic Vernier Structure. *J Am Chem Soc* **2005**, *127* (43), 15000–15001. https://doi.org/10.1021/ja055757a.

(30) Embrechts, H.; Kriesten, M.; Hoffmann, K.; Peukert, W.; Hartmann, M.; Distaso, M. Elucidation of the Formation Mechanism of Metal-Organic Frameworks via in-Situ Raman and FTIR Spectroscopy under Solvothermal Conditions. *Journal of Physical Chemistry C* **2018**, *122* (23), 12267–12278. https://doi.org/10.1021/acs.jpcc.8b02484.

(31) Lee, T.; Chang, Y. H.; Lee, H. L. Crystallization Process Development of Metal-Organic Frameworks by Linking Secondary Building Units, Lattice Nucleation and Luminescence: Insight into Reproducibility. *CrystEngComm* **2017**, *19* (3), 426–441. https://doi.org/10.1039/c6ce02246d.

(32) Kollias, L.; Cantu, D. C.; Glezakou, V. A.; Rousseau, R.; Salvalaglio, M. On the Role of Enthalpic and Entropic Contributions to the Conformational Free Energy Landscape of MIL-101(Cr) Secondary Building Units. *Adv Theory Simul* **2020**, *3* (12). https://doi.org/10.1002/adts.202000092.

(33) Malyarik, M. A.; Petrosyants, S. P.; Ilyukhin, A. B.; Buslaev, Yu. A. Denticity of the Nitrate Group and Coordination Number of Trivalent Indium in Nitrate Complexes. *Zhurnal Neorganicheskoi Khimii* **1993**, *38* (12), 1975–1980.

(34) Kozhevnikova, G. V. *The State of Indium Ions in Nitrate Solutions: A Raman Spectroscopic Study and GABOR KERESZTURY*; 1985; Vol. 98.